Numerical Tests of Approximations used in Theories for Cosmic Ray Transport

by

Victor Arendt

A Thesis submitted to the Faculty of Graduate Studies of
The University of Manitoba
in partial fulfillment of the requirements of the degree of

MASTER OF SCIENCE

Department of Physics and Astronomy
University of Manitoba
Winnipeg

Abstract

One of the challenges in astrophysics is describing the motion of cosmic rays in chaotic magnetic fields. I present a qualitative analysis of results from simulations of the motion of cosmic rays in axisymmetric turbulent magnetic fields. A test-particle code was employed using a modified sympletic integration method to calculate the particle trajectories. From the trajectories we calculate the diffusion coefficients along and across the mean field, the particle densities, as well as the particle's characteristic function and the exact and approximate fourth order velocity correlations which are important in analytical theories describing particle transport across the mean field. We show that having several definitions for the diffusion coefficient can provide insight into the behaviour of those diffusion coefficients as $t \to \infty$. We also show that for early times the parallel characteristic function does not take the form of a Gaussian distribution as assumed in several theories.

Acknowledgements

I would like to thank the following people ...

My supervisor, Dr. Andreas Shalchi, for taking me on as graduate student, and for the advice and clarifications he gave.

Dr. Jason Fiege, for the advice and discussions on computational methods.

Maiko Langelaar, for his help with all the IT issues encountered.

Erica Franzmann, for loaning the computational servers she normally used so I could finish the remaining simulations in time to include them in this work.

The physics department office for their support and assistance.

Erica Franzmann, Dr. Adam Rogers, Dr. Andreas Shalchi, and Lawrence Arendt for proofreading this document.

Contents

List of Figures

List of Tables

Chapter 1

Introduction

Spread between the stars are clouds of dust, plasma, and magnetic fields, interacting with and shaping each other as defined by the laws of magnetohydrodynamics. In addition to this, cosmic rays can be found: charged energetic particles, such as protons and electrons, that can and will interact with the magnetic fields that permeate space. These particles may have originated from stars via coronal mass ejection driven shocks, produced by supernovae via diffusive shock acceleration (Malkov and Drury, 2001), or from active galactic nuclei (Kronberg and Lovelace, 2015, Pierre Auger Collaboration et al., 2007).

As cosmic rays move through space, they are subjected to a force by the magnetic fields that permeate region of space the particles are traversing. The relativistic equation for the Lorentz force, $\vec{F}$, the particles experience is given by (in cgs units)

$$\vec{F}(\vec{x}(t),t) = m\frac{\mathrm{d}\gamma\vec{v}}{\mathrm{d}t} = q\left(\vec{E}(\vec{x}(t),t) + \frac{\vec{v}(t)}{c} \times \vec{B}(\vec{x}(t),t)\right). \tag{1.1}$$

Equation 1.1 describes the influence of the electric field $\vec{E}(\vec{x}(t),t)$ and the magnetic field $\vec{B}(\vec{x}(t),t)$ at time t on a particle at position $\vec{x}(t)$ with charge q, mass m, velocity

$\vec{v}(t)$, and Lorentz factor γ. In the simulations run for this thesis, the electric field was set to zero for all times and positions, which allows equation 1.1 to be rewritten as

$$\vec{F}(\vec{x}(t), t) = \gamma m \frac{\mathrm{d}\vec{v}}{\mathrm{d}t} = q\frac{\vec{v}(t)}{c} \times \vec{B}(\vec{x}(t), t). \tag{1.2}$$

Equation 1.2 also takes into account the fact that magnetic fields only affect the orientation of the velocity vector, not the magnitude, by removing γ from the time derivative. If the magnetic field the particles interact with were a uniform, time independent field, the resulting particle trajectory would be a helix centered on an axis parallel to the magnetic field. No further work would be required, as we would be able to calculate the classical trajectory of all particles in the system for all time, ignoring any particle-particle interactions.

However, the magnetic fields that cosmic rays interact with are not uniform, and in general the trajectories cannot be solved analytically for all times. As such, we need models to describe the magnetic field, and theories are needed to calculate the transport of ensembles of particles within a model. The types of magnetic field models that this thesis is concerned with are those that can be described by a combination of a uniform background field (or mean field), B_0, and a turbulent field, $\delta\vec{B}(\vec{x}, t)$. For simplicity we orientate the coordinate system so that the mean field is along the z axis, and the magnetic field is given by

$$\vec{B}(\vec{x}, t) = B_0\hat{z} + \delta\vec{B}(\vec{x}, t). \tag{1.3}$$

Understanding the behaviour and diffusion of these particles is crucial for studying problems such as the transport of particles in the solar corona (Fletcher, 1997) or exploring solar energetic particles (Dröge, 2000) for example. Over time, various theories have been proposed for calculating how particles diffuse in a magnetic field, with each theory having its own set of assumptions and approximations required to make the theory solvable (see, e.g., Shalchi (2009) for a review). One of the first theories for describing particle transport was the quasi-linear theory (Jokipii, 1966) or QLT. Effectively a perturbation theory, QLT evaluates the equations relating the diffusion coefficient to the magnetic correlation tensor using the unperturbed particle trajectories. While the theory describes parallel transport quite well in some cases, it fails to describe transport perpendicular to the mean field in all cases (Shalchi, 2009). This has lead to the development of other theories, such as the Non-Linear Guiding Center (NLGC) theory of Matthaeus et al. (2003) and the Unified Non-Linear Transport (UNLT) theory of Shalchi (2010) and its time dependent counterpart (Shalchi, 2017, Lasuik and Shalchi, 2017a). These more advanced theories still have assumptions and approximations required, however, and they should be tested against numerical simulations of particle trajectories to check their validity.

I have developed computer code in *C++* and *MATLAB* to simulate particle trajectories in magnetic turbulence. The simulation code is heavily based on the code used for Hussein et al. (2015) and Heusen (2017), with several modifications. As a starting point, the method of integration was replaced with a modified symplectic method (Section 3.4). I also developed code to calculate several additional quantities. The primary goals of this thesis are to

- Calculate the parallel and perpendicular diffusion coefficients for various magnetic field models and particle velocities.

- Compute the distribution of particles along the x, y, and z axes at various points in time and qualitatively compare the results to a Gaussian distribution.

- Calculate the Fourier transform of the particle distribution in spherical coordinates and qualitatively compare it to a Gaussian distribution.

- Calculate the velocity correlation as a function time, as well as the Fourier transform of the velocity correlation as a function of time and position to determine whether or not the approximations used in analytical theories are valid.

Chapter 2

Theory

In order to compare results from numerical simulation to theory, we must have a model or a set of models to use. The magnetic field models used throughout this work are the *slab* model, the *2D* model, and the *two component* or *composite* model. This final model is used to approximate the solar wind at 1 AU (Matthaeus et al., 1990, Bieber et al., 1996), and is a combination of the slab and 2D models. Each of these models is defined by its magnetic correlation tensor (see equations 2.11 and 2.16). On the theoretical side, the Non-Linear Guiding Center (NLGC) theory (Matthaeus et al., 2003) and the Unified Non Linear Transport (UNLT) theory (Shalchi, 2010, 2017, Lasuik and Shalchi, 2017a) are used as the comparison points. The summary of the magnetic correlation tensor and the various magnetic models is based on the material presented in *Nonlinear Cosmic Ray Diffusion Theories* by Shalchi (2009).

2.1 Theories For Describing Diffusion

Over time, various theories have been introduced to analytically calculate the diffusion coefficients for particle transport in magnetic turbulence, such as Quasi-Linear Theory (QLT) (Jokipii, 1966), the Non-Linear Guiding Center (NLGC) theory (Matthaeus et al., 2003), and the Unified Non-Linear Transport (UNLT) theory (Shalchi, 2010, 2017, Lasuik and Shalchi, 2017a,b). For a more in depth look at the first two theories listed (among others), see Nonlinear Cosmic Ray Diffusion Theories by Shalchi (2009). These theories rely on the Taylor-Green-Kubo (TGK) (Taylor, 1922, Green, 1951, Kubo, 1957) formulation and the Fokker-Planck equations to calculate the diffusion coefficients. A brief summary of the results from the TGK formulation and the Fokker-Planck equations will be given here.

2.1.1 Mathematical Definition of the Diffusion Coefficient

In order to discuss various diffusion theories, we first need to define the diffusion coefficient. To begin with, we have the particle mean square displacement

$$\Big\langle (\Delta x)^2 \Big\rangle (t) = \Big\langle (x(t) - x(0))^2 \Big\rangle, \tag{2.1}$$

where $\langle \cdots \rangle$ is the ensemble average operator. If we assume that the mean square displacement can be written as

$$\Big\langle (\Delta x)^2 \Big\rangle (t) \propto t^{\sigma}, \tag{2.2}$$

we can define several possible regimes as follows:

- $0 \leq \sigma < 1$ is sub-diffusion, and is identified by a decreasing diffusion coefficient;

- $\sigma = 1$ is normal diffusion, with diffusion coefficient constant in time;

- $1 < \sigma < 2$ is super-diffusion, and is identified by an increasing diffusion coefficient;

- $\sigma = 2$ is ballistic motion.

Given the presense of magnetic fields, we do not expect ballistic motion, rather it is assumed that the particles will in general follow the magnetic field lines (Matthaeus et al., 2003). The running diffusion coefficient can be defined as

$$\kappa_{ii} = \frac{\left\langle (\Delta x_i)^2 \right\rangle (t)}{2t} \tag{2.3a}$$

or

$$\kappa_{ii} = \frac{1}{2}\frac{\mathrm{d}}{\mathrm{d}t}\left\langle (\Delta x_i)^2 \right\rangle (t). \tag{2.3b}$$

If the collective behaviour of the particles becomes diffusive, then the two definitions in equation 2.3 will become equal when $t = \infty$.

2.1.2 TGK Formulation

The TGK formulation states that the mean square displacement can be calculated as

$$\left\langle (\Delta x_i)^2 \right\rangle (t) = \left\langle \left(\int_0^t \mathrm{d}t' v_i(t') \right)^2 \right\rangle \tag{2.4}$$

Under the assumption of homogeneity in time for the velocity, equation 2.4 can be rearranged, as shown in Shalchi (2009), to give

$$\kappa_{ii}(t) = \int_0^t \mathrm{d}t' \Big\langle v_i(t')v_i(0) \Big\rangle. \tag{2.5}$$

The integrand in equation 2.5 is defined as the velocity correlation function,

$$V_{ii}(t) = \Big\langle v_i(t')v_i(0) \Big\rangle. \tag{2.6}$$

2.1.3 Fokker-Planck Equation

In some analytical theories, the parallel transport of the particles is calculated via the Fokker-Planck equation. In two dimensions this equation (see Schlickeiser, 2002) reads

$$\frac{\partial f}{\partial t} + v\mu \frac{\partial f}{\partial z} = \frac{\partial}{\partial \mu}\left(D_{\mu\mu} \frac{\partial f}{\partial \mu} \right), \tag{2.7}$$

where $D_{\mu\mu}$ is the pitch-angle diffusion coefficient, μ is the pitch-angle cosine given by $\mu = v_z/v$, and $f = f(\mu, z, t)$ is the particle distribution function. By the Sturm-Liouville theorem, the function becomes isotropic after a sufficient period of time:

$$f(\mu, z, t \to \infty) \to \rho(z, t). \tag{2.8}$$

For $t \to \infty$, the pitch angle averaged function satisfies the diffusion equation (see Shalchi, 2009)

$$\frac{\partial \rho}{\partial t} = -\kappa_{zz} \frac{\partial^2 \rho}{\partial z^2}. \tag{2.9}$$

The solution to this equation for sharp inital conditions ($\rho(z,0) = \delta(z)$) is

$$\rho(z,t) = \frac{1}{\sqrt{4\pi\kappa_{\|}t}} e^{-\frac{z^2}{4\kappa_{\|}t}}. \tag{2.10}$$

The "sharp initial conditions" condition can be satisfied in simulations by replacing z with $\Delta z = z(t) - z(0)$, or more generally replacing $\vec{x}$ with $\Delta\vec{x} = \vec{x}(t) - \vec{x}(0)$.

2.2 Magnetic Correlation Tensor

One of the primary quantities in analytical theories is the magnetic correlation tensor. In physical space the tensor is written as

$$R_{lm}(\vec{x}, t, \vec{x}_0, t_0) = \left\langle \delta B_l(\vec{x}, t) \delta B_m^*(\vec{x}_0, t_0) \right\rangle, \tag{2.11}$$

where $\delta B_\mu(\vec{x}, t)$ is the turbulent magnetic field at position $\vec{x}$ and time t. Since it is often convenient to use Fourier space to calculate the tensor, we calculate the turbulent field as

$$\delta B_l(\vec{x}, t) = \int \mathrm{d}^3k \, \delta B_l(\vec{x}, t) e^{i\vec{k}\vec{x}}. \tag{2.12}$$

This leads to the correlation tensor being defined as

$$R_{lm}(\vec{x}, t, \vec{x}_0, t_0) = \left\langle \int \mathrm{d}^3k \int \mathrm{d}^3k' \, \delta B_l(\vec{k}, t) \delta B_m^*(\vec{k}', t_0) e^{i(\vec{k}\vec{x} - \vec{k}'\vec{x}_0)} \right\rangle. \tag{2.13}$$

We can now move the integral operator outside the ensemble average, yielding

$$R_{lm}(\vec{x}, t, \vec{x}_0, t_0) = \int \mathrm{d}^3k \int \mathrm{d}^3k' \left\langle \delta B_l(\vec{k}, t) \delta B_m^*(\vec{k}', t_0) e^{i(\vec{k}\vec{x} - \vec{k}'\vec{x}_0)} \right\rangle. \tag{2.14}$$

If $\vec{x}_0$ and $\vec{x}$ are particle positions, we invoke *Corrsin's Independence Hypothesis* (Corrsin, 1959), also called the *random phase approximation*, to separate the ensemble average into

$$\left\langle \delta B_l(\vec{k},t)\delta B_m^*(\vec{k}',t_0)e^{i(\vec{k}\vec{x}-\vec{k}'\vec{x}_0)}\right\rangle = \left\langle \delta B_l(\vec{k},t)\delta B_m^*(\vec{k},t)\right\rangle\left\langle e^{i(\vec{k}\vec{x}-\vec{k}'\vec{x}_0)}\right\rangle. \tag{2.15}$$

Since we are only considering static homogeneous turbulence, the field component can be written as

$$\left\langle \delta B_l(\vec{k},t)\delta B_m^*(\vec{k}',t_0)\right\rangle = P_{lm}(\vec{k})\delta(\vec{k}-\vec{k}'). \tag{2.16}$$

Integrating over k' results in

$$R_{lm}(\vec{x},t,\vec{x}_0,t_0) = \int \mathrm{d}^3k\, P_{lm}(\vec{k})\left\langle e^{i\vec{k}(\vec{x}-\vec{x}_0)}\right\rangle. \tag{2.17}$$

Here, we can see that the result depends only on the displacement $\Delta\vec{x} = \vec{x} - \vec{x}_0$, and since there is no explicit time dependence we can set $t_0 = 0$. In terms of particles, we can identify the remaining ensemble averaged quantity as the Fourier transform of the particle displacement distribution, also referred to as the characteristic function, given by

$$\left\langle e^{i\vec{k}\Delta\vec{x}}\right\rangle = \int_{\mathbb{V}} \mathrm{d}^3x\, \rho(\Delta\vec{x},t)e^{i\vec{k}\vec{x}} = \tilde{\rho}(\vec{k},t). \tag{2.18}$$

The characteristic function is a key input for analytical theories, as will be shown later.

2.3 Analytical Synthetic Turbulence Models

As mentioned previously, three models for the magnetic turbulence were used: the slab model, the 2D model, and the composite model. In each of these models, the background magnetic field is oriented along the z axis, and the magnetic turbulence is only in the $x-y$ plane. In the slab model, the turbulence magnitude depends only on the position along the z axis, with the field orientation completely independent of the wave orientation. On the other hand, the 2D model amplitude depends on the position in the $x-y$ plane, resulting in a field orientation that depends on the associated wave orientation. The composite model is assumed to be a linear combination of the slab and 2D models. The overall magnetic field used is a combination of these turbulent fields and a background or mean field $B_0\hat{z}$. The equation for this field is then

$$\vec{B} = B_0\hat{z} + db\,\delta\vec{B}(\vec{x}), \tag{2.19}$$

where $\delta\vec{B}(\vec{x})$ is the turbulent field used in the correlation tensor, while db controls the strength of the turbulent field allowing us to set $\frac{1}{\mathbb{V}}\int_{\mathbb{V}} \delta B^2 \, \mathrm{d}^3x = 1$. Since the models used are axisymmetric with respect to the z-axis we can write the wave vectors as

$$\vec{k} = k_{\parallel}\hat{z} + k_{\perp}\hat{k}_{\perp}, \tag{2.20}$$

and the diffusion coefficients as

$$\kappa_{\parallel} = \kappa_{zz} \tag{2.21}$$

and

$$\kappa_{\perp} = \kappa_{xx} = \kappa_{yy}. \tag{2.22}$$

An alternative method of defining the perpendicular diffusion coefficient is

$$\kappa_\perp = \frac{\kappa_{xx} + \kappa_{yy}}{2}, \tag{2.23}$$

which is the method used in this thesis.

2.3.1 Slab Turbulence

For the slab model the magnetic correlation tensor is defined as

$$P_{lm}^{slab}(\vec{k}) = g^{slab}(k_\parallel)\frac{\delta(k_\perp)}{k_\perp}\delta_{lm}, \tag{2.24}$$

with $l, m = x, y$ and $P_{zz} = P_{zm} = P_{lz} = 0$. The function $g^{slab}(k_\parallel)$ is the spectral function defining the amount of magnetic energy associated with each wave vector. In this thesis we used a spectrum given by

$$g^{slab}(k_\parallel) = \frac{C(s)}{2\pi}\delta B_{slab}^2 l_{slab}\frac{1}{\left(1 + (k_\parallel l_{slab})^2\right)^{\frac{s}{2}}}, \tag{2.25}$$

as proposed by Bieber et al. (1994). Here l_{slab} is the bend over scale for the spectrum, marking the transition from the energy range at small wave numbers to the inertial range at large wave numbers, and s is the inertial spectral index. The spectral function is normalized so that

$$\delta B_{slab}^2 = \delta B_x^2 + \delta B_y^2 = \int \mathrm{d}k\,(P_{xx} + P_{yy}). \tag{2.26}$$

The function $C(s)$ comes from the normalization of the spectrum, and is given by

$$C(s) = \frac{\Gamma\left(\frac{s}{2}\right)}{2\sqrt{\pi}\Gamma\left(\frac{s-1}{2}\right)}, \tag{2.27}$$

where $\Gamma(\cdots)$ is the gamma function.

2.3.2 Two Dimensional Turbulence

The two dimensional (2D) correlation tensor has the form

$$P_{lm}^{2D}(\vec{k}) = g^{2D}(k_\perp)\frac{\delta(k_\parallel)}{k_\perp}\left(\delta_{lm} - \frac{k_l k_m}{k_\perp^2}\right), \tag{2.28}$$

again with $l, m = x, y$ and $P_{zz} = P_{zm} = P_{lz} = 0$. At first glance the tensor appears to have non-zero off diagonal element, upon integration however, the off diagonal elements reduce to zero. The spectrum used for $g^{2D}(k_\perp)$ is

$$g^{2D}(k_\perp) = \frac{2D(s,q)}{\pi}\delta B_{2D}^2 l_{2D}\frac{(k_\perp l_{2D})^q}{(1+(k_\perp l_{2D})^2)^{\frac{(s+q)}{2}}}, \tag{2.29}$$

as proposed by Shalchi and Weinhorst (2009). Here, l_{2D} is the bend over scale for this model, s is the inertial spectral index, and the new parameter q is the energy spectral index. Using the normalization method from equation 2.26, we obtain the normalization factor $D(s,q)$ as

$$D(s,q) = \frac{\Gamma\left(\frac{s}{2}\right)}{2\Gamma\left(\frac{q+1}{2}\right)\Gamma\left(\frac{s-1}{2}\right)}. \tag{2.30}$$

Comparing equations 2.27 and 2.30 it can be seen that $C(s) = D(s, q = 0)$.

2.3.3 Composite Turbulence

As mentioned at the top of this section, the composite model is a linear combination of the slab and 2D models. The correlation tensor is therefore

$$P_{lm}^{Comp}(\vec{k}) = P_{lm}^{Slab}(\vec{k}) + P_{lm}^{2D}(\vec{k}), \tag{2.31}$$

and the magnetic field is calculated by

$$\delta\vec{B}_{Comp} = db_{slab}\delta\vec{B}_{Slab} + db_{2D}\delta\vec{B}_{2D}. \tag{2.32}$$

The values of db_{slab} and db_{2D} are given such that $db_{slab}^2 + db_{2D}^2 = 1$. With each of the turbulence components being normalized so that $\frac{1}{\mathbb{V}}\int_{\mathbb{V}} \delta B_{Slab}^2 \,\mathrm{d}^3x = \frac{1}{\mathbb{V}}\int_{\mathbb{V}} \delta B_{2D}^2 \,\mathrm{d}^3x = 1$, the overall strength of the turbulence is still controlled by db from equation 2.19. In addition to the variable strengths of each of the models, we can also consider variable length scales for each model. In these cases we change the ratio of l_{2D}/l_{Slab} by varying the value of l_{2D}.

2.4 Analytical Calculations of Diffusion Coefficients

2.4.1 Parallel Transport

As stated in equation 2.5, the running diffusion coefficient can be calculated as

$$\kappa_{ii} = \int_0^t \mathrm{d}t' \Big\langle v_i(t')v_i(0) \Big\rangle. \tag{2.33}$$

From the diffusion coefficient, we can get the parallel and perpendicular mean free paths, $\lambda_\parallel$ and $\lambda_\perp$ respectively, by

$$\lambda_\parallel = \frac{3\kappa_\parallel}{v} \tag{2.34}$$

$$\lambda_\perp = \frac{3\kappa_\perp}{v}. \tag{2.35}$$

The parallel mean free path can also be calculated from the pitch angle diffusion coefficient $D_{\mu\mu}(\mu)$ by Earl (1974)

$$\lambda_\parallel = \frac{3\kappa_\parallel}{v} = \frac{3v}{8}\int_{-1}^{+1} \mathrm{d}\mu \frac{(1-\mu^2)^2}{D_{\mu\mu}(\mu)}, \tag{2.36}$$

or by solving the Fokker-Planck equation for a time dependent diffusion coefficient.

2.4.2 Perpendicular Transport

For particle transport perpendicular to the mean field, a nonlinear theory such as NLGC theory (Matthaeus et al., 2003) or UNLT theory (Shalchi, 2010) is required. For these theories, the starting assumption is that the perpendicular guiding center velocity can be given by

$$\vec{v}_x(t) = a\vec{v}_z(t)\frac{\delta\vec{B}_x(\vec{x}(t),t)}{B_0}, \tag{2.37}$$

where a is an unknown parameter. Combining this with the TGK formulation from equation 2.5 yields

$$\kappa_\perp = \frac{a^2}{B_0^2}\int_0^\infty \mathrm{d}t \left\langle v_z(t)v_z(0)\delta B_x\big(\vec{x}(t),t\big)\delta B_x\big(\vec{x}(0),0\big)\right\rangle. \tag{2.38}$$

Using the equation for the magnetic field as a Fourier transform yields

$$\kappa_\perp = \frac{a^2}{B_0^2} \int_0^\infty \mathrm{d}t \int \mathrm{d}^3k \int \mathrm{d}^3k' \left\langle v_z(t) v_z(0) \delta B_x\left(\vec{k}\right) \delta B_x\left(\vec{k}'\right) e^{i(\vec{k}\vec{x}(t) - \vec{k}'\vec{x}(0))} \right\rangle. \tag{2.39}$$

In the above equation, we have dropped the time dependence from the fields, as we are only using static turbulence. The fourth order correlation is then approximated using Corrsin's hypothesis (Corrsin, 1959)

$$\left\langle v_z(t) v_z(0) \delta B_x\left(\vec{k}\right) \delta B_x\left(\vec{k}'\right) e^{i(\vec{k}\vec{x}(t) - \vec{k}'\vec{x}(0))} \right\rangle = \left\langle \delta B_x\left(\vec{k}\right) \delta B_x\left(\vec{k}'\right) \right\rangle \left\langle v_z(t) v_z(0) e^{i(\vec{k}\vec{x}(t) - \vec{k}'\vec{x}(0))} \right\rangle. \tag{2.40}$$

Since the turbulence is homogeneous, the quantity $\left\langle \delta B_x\left(\vec{k}\right) \delta B_x\left(\vec{k}'\right) \right\rangle$ can be replaced with $P_{xx}(\vec{k})\delta(\vec{k} - \vec{k}')$, yielding

$$\kappa_\perp = \frac{a^2}{B_0^2} \int_0^\infty \mathrm{d}t \int \mathrm{d}^3k \, P_{lm}(\vec{k}) \left\langle v_z(t) v_z(0) e^{i(\vec{k}\vec{x}(t) - \vec{k}'\vec{x}(0))} \right\rangle. \tag{2.41}$$

A point of difference between NLGC theory and UNLT theory is what happens with the correlation $\langle v_z(t) v_z(0) e^{i(\vec{k}\vec{x}(t) - \vec{k}'\vec{x}(0))} \rangle$. The UNLT theory attempts to calculate this quantity from the Fokker-Planck equation, while the NLGC theory approximates the correlation as

$$\left\langle v_z(t) v_z(0) e^{i(\vec{k}\vec{x}(t) - \vec{k}'\vec{x}(0))} \right\rangle = \left\langle v_z(t) v_z(0) \right\rangle \left\langle e^{i(\vec{k}\vec{x}(t) - \vec{k}'\vec{x}(0))} \right\rangle, \tag{2.42}$$

where the parallel second order velocity correlation function is given by

$$\left\langle v_z(t) v_z(0) \right\rangle = \frac{v^2}{3} e^{-\frac{vt}{\lambda_\parallel}} = \frac{v^2}{3} e^{-\frac{v^2 t}{3\kappa_\parallel}}, \tag{2.43}$$

and the characteristic function is

$$\left\langle e^{i\vec{k}\Delta\vec{x}} \right\rangle = e^{-\kappa_\parallel k_\parallel^2 t - \kappa_\perp k_\perp^2 t}. \tag{2.44}$$

The second order velocity correlation (2.43) is the velocity correlation that appears in the calculation $\kappa_\parallel$, and the equation for it is a result of the assumption that parallel transport assymptotically approaches diffusion. The characteristic function (2.44) is the Fourier transform of the particle distribution in physical space and the assumption of diffusive behaviour, as a Gaussian is the solution for a diffusion equation.

Chapter 3

Computational Implementation

3.1 Derivation of Unitless Quantities

In order to make all quantities unitless, as is preferred in numerical work, we start with the most general equations of motion for the system:

$$\frac{\mathrm{d}\vec{p}}{\mathrm{d}t} = q\left(\vec{E}(\vec{x}) + \frac{\vec{v}}{c} \times \vec{B}(\vec{x})\right), \tag{3.1a}$$

$$\frac{\mathrm{d}\vec{x}}{\mathrm{d}t} = \vec{v}, \tag{3.1b}$$

$$\vec{p} = \gamma m \vec{v}. \tag{3.1c}$$

Since we are concerned with systems that consist only of magnetic fields, $\vec{E}(\vec{x}) = 0$ for all values of $\vec{x}$. In the absence of any electric fields, momentum $|\vec{p}|$ is also conserved, allowing equations 3.1a and 3.1c to be combined and rearranged into

$$\frac{\mathrm{d}\vec{v}}{\mathrm{d}t} = \frac{q}{\gamma mc}\vec{v} \times \vec{B}(\vec{x}). \tag{3.2}$$

At this point, we introduce the scale factor for the total magnetic field B_0, such that $\vec{B}(\vec{x}) = B_0\vec{b}(\vec{x})$. The factor B_0 is defined by the following equations:

$$B_0 = \left| \frac{1}{\mathbb{V}} \int\limits_{\mathbb{V}} \vec{B}(\vec{x})\, \mathrm{d}^3x \right| \tag{3.3a}$$

or

$$B_0 = \sqrt{\frac{1}{\mathbb{V}} \int\limits_{\mathbb{V}} B^2(\vec{x})\, \mathrm{d}^3x}. \tag{3.3b}$$

Equation 3.3a is used if there is a background mean field, and equation 3.3b is used if there is no background mean field. Combining the equations of motion and the magnetic field scaling equation yields

$$\frac{\mathrm{d}\vec{v}}{\mathrm{d}t} = \frac{qB_0}{\gamma mc}\vec{v} \times \vec{b}(\vec{x}). \tag{3.4}$$

Recognizing that $\frac{qB_0}{\gamma mc}$ is the relativistic gyrofrequency Ω for a particle in a uniform magnetic field of strength B_0, we define a unitless time τ as

$$\tau = \Omega t, \tag{3.5a}$$

along with the associated replacement derivatives

$$\frac{\mathrm{d}}{\mathrm{d}t} = \frac{\mathrm{d}\tau}{\mathrm{d}t}\frac{\mathrm{d}}{\mathrm{d}\tau} = \Omega\frac{\mathrm{d}}{\mathrm{d}\tau}, \tag{3.5b}$$

and the time-differential

$$\mathrm{d}t = \frac{1}{\Omega}\mathrm{d}\tau. \tag{3.5c}$$

We also introduce, length scale ℓ_0, with which we can define a unitless position by

$$\vec{\chi} = \frac{\vec{x}}{\ell_0}, \tag{3.6a}$$

with corresponding derivative

$$\frac{\mathrm{d}}{\mathrm{d}x_i} = \frac{1}{\ell_0}\frac{\mathrm{d}}{\mathrm{d}\chi_i} \tag{3.6b}$$

and differential element

$$\mathrm{d}x_i = \ell_0 \mathrm{d}\chi. \tag{3.6c}$$

For simulation purposes, the length scale is set to the bend over scale l_{Slab}. Combining equations 3.5 and 3.6 with the equations of motion, we get

$$\Omega\frac{\mathrm{d}\vec{v}}{\mathrm{d}\tau} = \Omega\vec{v} \times \vec{b}(\vec{\chi}), \qquad \Omega\ell_0\frac{\mathrm{d}\vec{\chi}}{\mathrm{d}\tau} = \vec{v}, \tag{3.7}$$

from which we can see that the velocity must be made unitless by

$$\vec{R} = \frac{\vec{v}}{\Omega\,\ell_0} = \frac{\gamma mc\vec{v}}{qB_0\ell_0}. \tag{3.8}$$

The choice of R as the variable for the unitless velocity comes from the fact that the magnetic rigidity, R_B, of a particle is defined as

$$R_B = \frac{pc}{q} = \frac{\gamma mcv}{q},$$

which contains the magnitude of the velocity. This means that $\vec{R}$ is also a unitless vector rigidity given by $\vec{R} = \vec{R}_B / B_0 \ell_0$. The unitless equations of motion now read

$$\frac{\mathrm{d}\vec{R}}{\mathrm{d}\tau} = \vec{R} \times \vec{b}(\vec{\chi}) \tag{3.9a}$$

$$\frac{\mathrm{d}\vec{\chi}}{\mathrm{d}\tau} = \vec{R} \tag{3.9b}$$

The only remaining quantity to make unitless is the wave vector used to define the magnetic turbulence. This is done by defining $\vec{k} = \vec{k}_{unitless} = \vec{k}_{units} \ell_0$, which allows us to use the spectrum functions in equations 2.25 and 2.29 to set $\ell_0 = l_{slab}$ or $\ell_0 = l_{2D}$ for pure slab or pure 2D turbulence, respectively. In the case of composite turbulence, we use $\ell_0 = l_{slab}$ and then introduce a new parameter $\ell = \frac{l_{2D}}{\ell_0}$ to define the ratio between the two length scales.

3.2 Generic Magnetic Turbulence Model

In order to solve the equations of motion, we start with equation 2.19. Since we are calculating the turbulence using a Fourier sum, the general equation for the magnetic turbulence is given by

$$\delta\vec{B} = \sqrt{2} B_0 \sum_{n=1}^{N} A(\vec{k}_n) \hat{\delta B}(\vec{k}_n) \cos(\vec{k}_n \vec{x} + \varphi_n). \tag{3.10}$$

In the above equation, $A(\vec{k}_n)$ is the amplitude associated with wave vector $\vec{k}_n$, $\hat{\delta B}(\vec{k}_n)$ is the unit vector for the field associated with $\vec{k}_n$, and φ_n is a random phase offset included to prevent all the waves from taking their maximum amplitude at $\vec{x}$. Once the equations have been scaled and combined to contain only unitless quantities and variables, we get

$$
\begin{aligned}
\vec{b} &= \hat{z} + db\,\delta\vec{b} \\
&= \hat{z} + db\sqrt{2}\sum_{n=1}^{N} A(\vec{k}_n)\delta\hat{B}(\vec{k}_n)\cos(\vec{k}_n\vec{\chi} + \varphi_n),
\end{aligned}
\tag{3.11}
$$

which is the equation that is used in the simulations. It should be noted that when scaling the wave numbers, the length scale ℓ only appears in the amplitude function for 2D turbulence, and does not add any additional scaling onto the particle position. In these cases, the magnetic turbulence equation reads

$$
\delta\vec{b}_{2D} = \sqrt{2}\sum_{n=1}^{N} A_{2D}(\ell\vec{k}_n)\delta\hat{B}_{2D}(\vec{k}_n)\cos(\vec{k}_n\vec{\chi} + \varphi_n).
\tag{3.12}
$$

Now that the turbulence has been defined in terms of a sum of cosine functions, we transform it into a sum of complex exponentials, which will be useful later on. The complex form of the equation reads as

$$
\begin{aligned}
\delta\vec{b}_{complex} = \sqrt{2}\sum_{n=1}^{N} & A(\vec{k}_n)\delta\hat{B}(\vec{k}_n) \\
& \times \left(\frac{e^{i(\vec{k}_n\vec{\chi}+\varphi_n)} + e^{-i(\vec{k}_n\vec{\chi}+\varphi_n)}}{2}\right).
\end{aligned}
\tag{3.13}
$$

Since our spectra, $g_{slab}(\vec{k})$ and $g_{2D}(\vec{k})$, only depend on the magnitude of the wave vector along the $\hat{z}$ axis or in the xy-plane, the wave number sum can be re-indexed. This is done by defining negative indices for the wave number and phase offset as $\vec{k}_{-n} = -\vec{k}_n$ and $\varphi_{-n} = -\varphi_n$ respectively. The magnetic field orientation must then be defined as $\delta\hat{B}(\vec{k}_{-n}) = \delta\hat{B}(\vec{k}_n)$. The magnetic turbulence sum can now be written as

$$\begin{aligned}
\delta\vec{b}_{complex} &= \frac{1}{\sqrt{2}}\sum_{n=1}^{N} A(\vec{k}_n)\delta\hat{B}(\vec{k}_n)e^{i(\vec{k}_n\vec{x}+\varphi_n)} \\
&+ \frac{1}{\sqrt{2}}\sum_{n=-N}^{-1} A(\vec{k}_n)\delta\hat{B}(\vec{k}_n)e^{i(\vec{k}_n\vec{x}+\varphi_n)} \\
&= \frac{1}{\sqrt{2}}\sum_{\substack{n=-N \\ n\neq 0}}^{N} A(\vec{k}_n)\delta\hat{B}(\vec{k}_n)e^{i(\vec{k}_n\vec{x}+\varphi_n)}. \qquad (3.14)
\end{aligned}$$

With the turbulence written as a sum of complex exponentials, it is relatively easy to find the Fourier transform. Specifically, we replace $e^{i(\vec{k}_n\vec{x}+\varphi_n)}$ with $e^{i\varphi_n}\delta^3(\vec{k}-\vec{k}_n)$ to get

$$\mathcal{F}(\delta\vec{b}) = \tilde{\delta\vec{b}} = \frac{1}{\sqrt{2}}\sum_{\substack{n=-N \\ n\neq 0}}^{N} A(\vec{k}_n)\delta\hat{B}(\vec{k}_n)e^{i\varphi_n}\delta^3(\vec{k}-\vec{k}_n). \qquad (3.15)$$

This equation will be used later when deriving the equation for the wave amplitudes.

3.3 Numerical Implementation of Magnetic Turbulence

In order to fully specify the turbulence at any given particle position, we need a set of wave vectors and a corresponding set of magnetic field vectors. Each of the magnetic field vectors can be separated into an amplitude and an orientation, while the wave vectors can be separated into wave numbers and orientation. The wave unit vector, amplitude, and field orientation all depend on the type of model being employed, while the wave numbers can depend on either the duration of the simulation or the equation for the field amplitude. We begin with the method of selecting the range of wave numbers used.

3.3.1 Wave Vector Range

There are two ways to determine the range of wave numbers used in a simulation. The first method uses the particle rigidity in combination with the maximum time τ_{max} that a particle is tracked for and the size of time step $\mathrm{d}\tau$ used, while the second method uses the amplitude to determine when a wave number no longer has a significant contribution to the overall magnetic field. The first method has the advantage of knowing that the wave numbers used will interact with the particles as they propagate, while at the same time possibly excluding wave numbers that would still have a sizable contribution to the overall field. Conversely, the second method will result in the inclusion of all wave numbers that have a sizable contribution to the overall field. Unfortunately this comes at the cost of possibly including waves that may have no noticeable change in phase over the course of the particle's trajectory, resulting an unwanted additional mean field. Having stated this, it must be noted that the two methods are not mutually exclusive. The first method is explored here, and the second method will be explored when dealing with the amplitude calculations later in this chapter.

When determining the minimum and maximum wave numbers, it is important to take into account whether or not a particle can interact with the wave number. When we say that a particle can or cannot interact with a wave number, we are referring to whether or not the particle will experience a noticeable or resolvable change in the magnetic field. Small wave numbers are noticeable if the maximum distance the particle can travel is enough to cause a noticeable change in the contribution to the field by said wave number, while large wave numbers are resolvable if they are smaller than the inverse of the discrete change in particle position per time step. This works out to

$$k_{min} = \frac{1}{R\tau_{max}} \qquad \text{and} \qquad k_{max} = \frac{1}{|R_i|\mathrm{d}\tau} \tag{3.16}$$

for the minimum and maximum wave numbers, respectively, where R_i is the component of the rigidity parallel to the wave vector.

Ideally, k_{min} should be slightly smaller than $\frac{1}{|\vec{R}|\tau_{max}}$ to avoid any potential box effects, and k_{max} should be exactly equal to $\frac{1}{R_i \mathrm{d}\tau}$ to result in a resolvable oscillating effect from the larger wave numbers. The first problem with this is that the value R_i can range from $-|\vec{R}|$ to $|\vec{R}|$, resulting in a maximum wave number with the range of $(|\vec{R}|\mathrm{d}\tau)^{-1} \leq k_{max} \leq \infty$. Furthermore, when comparing results for different rigidities, it is preferred to keep as many other parameters as constant as possible, making k_{min} dependent not on just the rigidity of the particles in the current simulation, but also the rigidity of the particles in any simulation we wish to compare the results to. To solve both of these problems we can incorporate the second method of using the amplitude to determine the cutoff. This will be done formally once the equation for the amplitude has been derived.

3.3.2 Wave Number Calculation

From the formulae for the minimum and maximum wave numbers, it can be seen that the range of wave numbers spans several orders of magnitude. There are several ways of generating the magnetic field using such a large range of wave numbers. The first is to pre-compute the field, either directly or by Fast Fourier Transform (FFT), and then interpolate the field onto the position of the particle. This requires a significant number (at least $2\frac{k_{max}}{k_{min}}+1$) of uniformly spaced wave vectors, and demands large amounts of memory to store the field values. Furthermore, the chaotic nature of the resulting turbulent field could be called into question by the act of interpolating, regardless of the interpolation method.

The method we use instead has the wave numbers spaced logarithmically, with the field calculated at the particle position exactly. This form of calculating the magnetic field is identical to the one described in Hussein et al. (2015), which in turn was compared against Tautz (2010). While this method is more computationally expensive, the field can be calculated more accurately with less memory required to do so. With this method, the wave numbers are given by

$$k_n = k_{n-1}c_k = k_{min}c_k^{n-1} \qquad n = 1, 2, 3, ..., N; \tag{3.17}$$

where c_k is a constant given by $c_k = e^{ln(k_{max}/k_{min})/(N-1)}$ or equivalently $c_k = \left(\frac{k_{max}}{k_{min}}\right)^{\frac{1}{N-1}}$. The spacing between the wave numbers can be calculated as

$$\begin{aligned} \mathrm{d}k_n &= k_n - k_{n-1} \\ &= k_n - k_n c_k^{-1} \\ &= k_n(1 - c_k^{-1}). \end{aligned} \tag{3.18}$$

Now that the wave numbers have been calculated, it is possible to discuss the amplitude calculations.

3.3.3 Amplitude Calculation

In order to derive the formula for the wave amplitude, we start with the magnetic correlation tensor from equation 2.16, and compare the analytical equation to one with our discrete turbulence. To start, we take the equation for the tensor and plug in our equation for the turbulence in Fourier space, resulting in

$$\begin{aligned}\left\langle \delta b_\mu(\vec{\chi})\delta b_\nu^*(\vec{\chi})\right\rangle &= \Bigg\langle \left(\int \mathrm{d}^3k \frac{1}{\sqrt{2}} \sum_{\substack{n_1=-N\\ n_1\neq 0}}^{N} A(\vec{k}_{n_1}) e^{i\varphi_{n_1}} \delta\hat{B}_\mu(\vec{k}_{n_1})\delta^3(\vec{k}-\vec{k}_{n_1}) e^{i\vec{k}\vec{\chi}}\right) \\ &\quad \times \left(\int \mathrm{d}^3k' \frac{1}{\sqrt{2}} \sum_{\substack{n_2=-N\\ n_2\neq 0}}^{N} A(\vec{k}_{n_2}) e^{-i\varphi_{n_2}} \delta\hat{B}_\nu(\vec{k}_{n_2})\delta^3(\vec{k}'-\vec{k}_{n_2}) e^{i\vec{k}'\vec{\chi}'}\right)\Bigg\rangle \\ &= \frac{1}{2}\sum_{\substack{n_1=-N\\ n_1\neq 0}}^{N}\sum_{\substack{n_2=-N\\ n_2\neq 0}}^{N} A(\vec{k}_{n_1})A(\vec{k}_{n_2})\Big\langle e^{i(\varphi_{n_1}-\varphi_{n_2})}\delta\hat{B}_\mu(\vec{k}_{n_1})\delta\hat{B}_\nu(\vec{k}_{n_2}) \\ &\quad \times \int \mathrm{d}^3k \int \mathrm{d}^3k' e^{i(\vec{k}\vec{\chi}-\vec{k}'\vec{\chi}')}\delta^3(\vec{k}-\vec{k}_{n_1})\delta^3(\vec{k}'-\vec{k}_{n_2})\Big\rangle. \end{aligned} \tag{3.19}$$

Here we have used the fact that the amplitude is not a function of any random variables in order to remove it from the ensemble average. To continue deriving the equation for the amplitude, we break apart the ensemble average using Corrsin's Independence Hypothesis (see Corrsin 1959) as we did in equation 2.15 to get

$$\begin{aligned}\left\langle \delta b_\mu(\vec{\chi})\delta b_\nu^*(\vec{\chi})\right\rangle &= \frac{1}{2}\sum_{\substack{n_1=-N\\ n_1\neq 0}}^{N}\sum_{\substack{n_2=-N\\ n_2\neq 0}}^{N} A(\vec{k}_{n_1})A(\vec{k}_{n_2})\left\langle e^{i(\varphi_{n_1}-\varphi_{n_2})}\right\rangle\left\langle \delta\hat{B}_\mu(\vec{k}_{n_1})\delta\hat{B}_\nu(\vec{k}_{n_2})\right\rangle \\ &\quad \times \left\langle \int \mathrm{d}^3k \int \mathrm{d}^3k' e^{i(\vec{k}\vec{\chi}-\vec{k}'\vec{\chi}')}\delta^3(\vec{k}-\vec{k}_{n_1})\delta^3(\vec{k}'-\vec{k}_{n_2})\right\rangle. \end{aligned} \tag{3.20}$$

We now calculate the ensemble average for the phase offset φ_n by

$$\left\langle e^{i(\varphi_{n_1}-\varphi_{n_2})}\right\rangle = \delta_{n_1 n_2}, \tag{3.21}$$

which allows us to set $n_1 = n_2 = n$. After integrating over $\vec{k}'$, the equation reduces to

$$\left\langle \delta b_\mu(\vec{\chi}) \delta b^*_\nu(\vec{\chi}) \right\rangle = \frac{1}{2} \sum_{\substack{n=-N \\ n\neq 0}}^{N} A^2(\vec{k}_n) \left\langle \delta\hat{B}_\mu(\vec{k}_n) \delta\hat{B}_\nu(\vec{k}_n) \right\rangle \\ \times \left\langle \int \mathrm{d}^3 k e^{i(\vec{k}\vec{\chi} - \vec{k}_n \vec{\chi}')} \delta^3(\vec{k} - \vec{k}_n) \right\rangle. \tag{3.22}$$

Equation 3.22 is the general equation for the magnetic correlation using our discrete turbulence, which we now compare to the analytic equation to get

$$\int \mathrm{d}^3 k P_{\mu\nu}(\vec{k}) \tilde{\rho}(\vec{k}, \Delta\vec{\chi}) = \frac{1}{2} \sum_{\substack{n=-N \\ n\neq 0}}^{N} A^2(\vec{k}_n) \left\langle \delta\hat{B}_\mu(\vec{k}_n) \delta\hat{B}_\nu(\vec{k}_n) \right\rangle \\ \times \left\langle \int \mathrm{d}^3 k e^{i(\vec{k}\vec{\chi} - \vec{k}_n \vec{\chi}')} \delta^3(\vec{k} - \vec{k}_n) \right\rangle. \tag{3.23}$$

At this point, we need to use a specific model to proceed with the derivation of the formula for the amplitude as a function of wave number. We use the slab and 2D models outlined in sections 2.3.1 and 2.3.2 to develop a general equation for the turbulence amplitude.

Slab Model Implementation

In the slab model the magnetic field orientation is completely independent of the wave vector orientation, meaning that the ensemble average over $\delta\hat{B}_\mu \delta\hat{B}_\nu$ reduces to $\frac{1}{2}\delta_{\mu\nu}$, while the integral over $\vec{k}$ reduces to an integral over $k_\parallel$. Replacing $P_{\mu\nu}(\vec{k})$ with

$P_{\mu\nu}^{slab}(\vec{k})$ from equation 2.24, we get

$$\begin{aligned}&2\pi\delta_{\mu\nu}\int \mathrm{d}k_{\|} g^{slab}(k_{\|})\tilde{\rho}(k_{\|},\Delta\vec{\chi})\\ =&\frac{1}{4}\delta_{\mu\nu}\sum_{\substack{n=-N\\ n\neq 0}}^{N} A^2(\vec{k}_n)\left\langle\int \mathrm{d}k_{\|} e^{i(\vec{k}_{\|}\vec{\chi}-\vec{k}_n\vec{\chi}')}\delta(k_{\|}-k_n)\right\rangle.\end{aligned} \tag{3.24}$$

Integration over $k_{\|}$ forces $k_{\|}=k_n$ and converts the integral on the left hand side of equation 3.24 into a summation given by

$$\int \mathrm{d}k_{\|} g^{slab}(k_{\|})\tilde{\rho}(k_{\|},\Delta\vec{\chi}) = \sum_{n=1}^{N} g^{slab}(k_n)\mathrm{d}k_n\tilde{\rho}(k_n,\Delta\vec{\chi}). \tag{3.25}$$

The differential element $\mathrm{d}k_n$ is kept in the equation, since $P_{\mu\nu}^{slab}(\vec{k})$ was normalized to $\frac{1}{2}\delta_{\mu\nu}$ by integration. On the right hand side of the equation we have the ensemble average of $e^{i\vec{k}_n\Delta\vec{\chi}}$, which is equal to $\tilde{\rho}(k_n,\Delta\vec{\chi})$ by equation 2.18. Since we assume the ensemble average to be symmetric about the origin, we can change the index n to go from one to N by multiplying both sides by two. Finally, we insert equation 2.25 to get

$$\begin{aligned}&\frac{1}{2}\delta_{\mu\nu}\sum_{\substack{n=-N\\ n\neq 0}}^{N} A^2(\vec{k}_n)\tilde{\rho}(k_{\|},\Delta\vec{\chi})\\ &= 4\pi\delta_{\mu\nu}\sum_{\substack{n=-N\\ n\neq 0}}^{N}\frac{C(s)}{2\pi}\frac{1}{(1+k_n^2)^{\frac{s}{2}}}\tilde{\rho}(k_{\|},\Delta\vec{\chi})\\ &= \frac{1}{2}\delta_{\mu\nu}\sum_{\substack{n=-N\\ n\neq 0}}^{N}\frac{2\Gamma\left(\frac{s}{2}\right)}{\sqrt{\pi}\Gamma\left(\frac{s-1}{2}\right)}\frac{1}{(1+k_n^2)^{\frac{s}{2}}}\tilde{\rho}(k_{\|},\Delta\vec{\chi})\mathrm{d}k_n.\end{aligned} \tag{3.26}$$

By comparing both sides of the equation, we can see that the amplitude is given by

$$A(\vec{k}_n) = \sqrt{\frac{2\Gamma\left(\frac{s}{2}\right)}{\sqrt{\pi}\Gamma\left(\frac{s-1}{2}\right)} \frac{1}{(1+k_n^2)^{\frac{s}{2}}} \mathrm{d}k_n}. \tag{3.27}$$

Since we do not use the full range of wave numbers ($0 \leq k \leq \infty$), and $\sum_{n=1}^{N} A^2(\vec{k}_n)$ must be equal to one, we calculate the amplitude as

$$A(\vec{k}_n) = \sqrt{\frac{G^{slab}(k_n, s)\mathrm{d}k_n}{\sum_{n=1}^{N} G^{slab}(k_n, s)\mathrm{d}k_n}}, \tag{3.28}$$

where $G^{slab}(k_n, s) = \frac{1}{(1+k_n^2)^{\frac{s}{2}}}$.

2D Model Implementation

For the 2D model, the field orientation vector $\delta\hat{B}(\vec{k})$ is given by a rotation of the wave vector by $\pm\pi/2$ in the $x - y$ plane. As such, we calculate the wave vector and corresponding field unit vector as

$$\begin{aligned}
\hat{k}_n &= \cos(\phi_n)\hat{x} + \sin(\phi_n)\hat{y} \\
\delta\hat{B}(\vec{k}_n) &= -\sin(\phi_n)\hat{x} + \cos(\phi_n)\hat{y} \\
&= -\frac{k_{y,n}}{k_n}\hat{x} + \frac{k_{x,n}}{k_n}\hat{y}
\end{aligned}$$

which is equivalent to a rotation of $\pi/2$. We can therefore write the product of $\delta\hat{B}_\mu(\vec{k}_n)$ and $\delta\hat{B}_\nu(\vec{k}_n)$ for $\mu, \nu = x, y$ as

$$\delta\hat{B}_\mu(\vec{k}_n)\delta\hat{B}_\nu(\vec{k}_n) = \delta_{\mu\nu} - \frac{k_{\mu,n}k_{\nu,n}}{k_n^2}. \tag{3.29}$$

Substituting this into equation 3.23 along with the equation for $P^{2D}_{\mu\nu}(\vec{k})$ (equation 2.28), we get

$$\begin{aligned}
&\int \mathrm{d}^3k \frac{2D(s,q)}{\pi}\frac{k_\perp^q}{(1+k_\perp^2)^{\frac{q+s}{2}}}\frac{\delta(k_\parallel)}{k_\perp}\left(\delta_{\mu\nu}-\frac{k_\mu k_\nu}{k_\perp^2}\right)\tilde{\rho}(\vec{k},\Delta\vec{\chi})\\
=&\frac{1}{2}\sum_{\substack{n=-N\\n\neq 0}}^{N} A^2(\vec{k}_n)\Big\langle\left(\delta_{\mu\nu}-\frac{k_{\mu,n}k_{\nu,n}}{k_n^2}\right)\Big\rangle\Big\langle\int \mathrm{d}^3k e^{i(\vec{k}\vec{\chi}-\vec{k}_n\vec{\chi}')}\delta^3(\vec{k}-\vec{k}_n)\Big\rangle.
\end{aligned} \tag{3.30}$$

The assumption required when using Corrsin's Approximation on 2D turbulence is that the characteristic function is independent of the orientation of the wave vector in the $x-y$ plane. Integration over k_z and k_ϕ on the left hand side therefore yields

$$\begin{aligned}
&\int \mathrm{d}^3k \frac{2D(s,q)}{\pi}\frac{k_\perp^q}{(1+k_\perp^2)^{\frac{q+s}{2}}}\frac{\delta(k_\parallel)}{k_\perp}\left(\delta_{\mu\nu}-\frac{k_\mu k_\nu}{k_\perp^2}\right)\tilde{\rho}(\vec{k},\Delta\vec{\chi})\\
=&\frac{1}{2}\delta_{\mu\nu}\int_0^\infty \mathrm{d}k_\perp 2D(s,q)\frac{k_\perp^q}{(1+k_\perp^2)^{\frac{q+s}{2}}}\tilde{\rho}(\vec{k}_\perp,\Delta\vec{\chi});
\end{aligned} \tag{3.31}$$

while integration over k_z and averaging over all posible field realizations on the right hand side yields

$$\frac{1}{4}\delta_{\mu\nu}\sum_{\substack{n=-N\\n\neq 0}}^{N} A^2(\vec{k}_n)\Big\langle\int \mathrm{d}k_x\mathrm{d}k_y e^{i(\vec{k}\vec{\chi}-\vec{k}_n\vec{\chi}')}\delta(k_x-k_{x,n})\delta(k_x-k_{x,n})\Big\rangle. \tag{3.32}$$

We recognize that the ensemble average of $\int \mathrm{d}k_x\mathrm{d}k_y e^{i(\vec{k}\vec{\chi}-\vec{k}_n\vec{\chi}')}\delta(k_x-k_{x,n})\delta(k_x-k_{x,n})$ is just the characteristic function from equation 2.18, and the act of integration converts the remaining left hand side integral into a sum over wave number magnitudes. The final result for the amplitude equation, after canceling shared terms and converting the sum on the left hand side to be from one to N, is then

$$\sum_{n=1}^{N} \frac{2\Gamma\left(\frac{q+s}{2}\right)}{\Gamma\left(\frac{q+1}{2}\right)\Gamma\left(\frac{s-1}{2}\right)} \frac{k_n^q}{(1+k_n^2)^{\frac{q+s}{2}}} \mathrm{d}k_n = \sum_{n=1}^{N} A^2(\vec{k}_n) \tag{3.33}$$

Using the same considerations we used for the slab turbulence regarding the normalization and spectrum cutoff, we calculate the amplitude for the 2D turbulence as

$$A(\vec{k}_n) = \sqrt{\frac{G^{2D}(k_n, q, s)\mathrm{d}k_n}{\sum_{n=1}^{N} G^{2D}(k_n, q, s)\mathrm{d}k_n}}, \tag{3.34}$$

where $G^{2D}(k_n, q, s) = \frac{k_n^q}{(1+k_n^2)^{\frac{q+s}{2}}}$.

General Application

It can be noted that the equation for the wave amplitude for both the slab and 2D models are very similar, specifically $G^{slab}(k_n, s) = G^{2D}(k_n, q = 0, s)$. We can therefore write a general formula for the wave amplitude as

$$A(\vec{k}_n) = \sqrt{\frac{G(k_n, q, s)\mathrm{d}k_n}{\sum_{n=1}^{N} G(k_n, q, s)\mathrm{d}k_n}}, \tag{3.35}$$

with

$$G(k_n, q, s) = \frac{k_n^q}{(1+k_n^2)^{\frac{q+s}{2}}}. \tag{3.36}$$

If we were using linearly spaced wave numbers, the factor of $\mathrm{d}k_n$ would drop out, leaving a simple expression for the amplitude. However, since we are using logarithmically spaced wave numbers, we can rearrange the equation as follows:

$$\begin{aligned}
G(k_n, q, s)\mathrm{d}k_n &= \frac{k_n^q \mathrm{d}k_n}{(1+k_n^2)^{\frac{q+s}{2}}} \\
&= \frac{k_n^q k_n (1+c_k^{-1})}{(1+k_n^2)^{\frac{q+s}{2}}} \\
&= \frac{k_n^{q+1}(1+c_k^{-1})}{(1+k_n^2)^{\frac{(q+1)+(s-1)}{2}}} \\
&= G(k_n, q+1, s-1)(1+c_k^{-1}). \qquad (3.37)
\end{aligned}$$

When the amplitude is calculated, the factor of $(1+c_k^{-1})$ cancels out, leaving us with

$$A(\vec{k}_n) = \sqrt{\frac{G(k_n, q+1, s-1)}{\sum_{n=1}^{N} G(k_n, q+1, s-1)}}. \qquad (3.38)$$

We can further simplify the equation by bringing the sqrt inside the numerator, resulting in

$$A(\vec{k}_n) = \frac{G(k_n, \frac{q+1}{2}, \frac{s-1}{2})}{\sqrt{\sum_{n=1}^{N} G(k_n, q+1, s-1)}}. \qquad (3.39)$$

We use equations 3.28 and 3.34 to calculate the amplitude in our simulations. However, we can use equation 3.39 to determine the general properties of the amplitude. For small values of k_n the amplitude goes as $k_n^{\frac{q+1}{2}}$, while for large values of k_n the amplitude goes as $k^{-\frac{s-1}{2}}$. The maximum of $G(k, q, s)$ can be found at $k_{peak} = \sqrt{\frac{q}{s}}$, which means the maximum amplitude occurs at $k = \sqrt{\frac{q+1}{s-1}}$. For the composite models with varying length scales, the 2D model has its peak given by $k = \frac{1}{\ell}\sqrt{\frac{q+1}{s-1}}$, where ℓ is the ratio of the slab and 2D bendover scales. Once the values of q and s are specified, we can determine whether our maximum and minimum wave numbers cover enough of the spectrum for specific models.

3.3.4 Summary of Turbulence Implementation and Specific Numerical Values

Parameter	*Slab*	*2D*
Wave Vector $\vec{k}_n$	$k_n\hat{z}$	$k_n \cos\phi_n \hat{x} + k_n \sin\phi_n \hat{y}$
k_{min}	10^{-5}	10^{-5}
k_{max}	10^{3}	10^{3}
ϕ_n	$0 \leq \phi_n \leq 2\pi$	$0 \leq \phi_n \leq 2\pi$
Number of Waves	256	256
Field Orientation $\hat{\delta B}(\vec{k}_n)$	$-\sin\phi_n\hat{x} + \cos\phi_n\hat{y}$	$-\sin\phi_n\hat{x} + \cos\phi_n\hat{y}$
Amplitude $A(k_n)$	$\sqrt{\frac{G(k_n,q,s)\mathrm{d}k_n}{\sum_{n=1}^{N} G(k_n,q,s)\mathrm{d}k_n}}$	$\sqrt{\frac{G(k_n,q,s)\mathrm{d}k_n}{\sum_{n=1}^{N} G(k_n,q,s)\mathrm{d}k_n}}$
Energy Spectral Index q	0	3
Inertial Spectral Index s	${}^{5}/_{3}$	${}^{5}/_{3}$
Phase Offset φ_n	$0 \leq \varphi_n \leq 2\pi$	$0 \leq \varphi_n \leq 2\pi$
Turbulence Strength db	variable	variable
Length Scale Ratio ℓ	N/A	1, 0.1

Table 3.1: Parameter implementation for slab and 2D turbulence. Composite turbulence is just a linear combination of the slab and 2D modes.

Table 3.1 lists the values of the parameters that were used in the simulations. When possible, the values or equations that defined the parameters were kept the same to simplify the simulation code. Figure 3.1 shows the cumulative sum of the discrete amplitude squared, equivalent to the normalized cumulative sum of the spectrum function. For the purpose of demonstrating that the choice of $k_{max} = 10^3$ is reasonable, we extended the spectrum with an additional 255 waves above and below the maximum and minimum values and then summed over all waves from k'_{min} to

k_n, with k'_{min} being the new minimum wave length. It can easily be seen from the graphs that the amount magnetic energy stored in wave numbers less than $k = 10^{-5}$ is insignificant, while the energy stored in wave numbers greater than $k = 10^5$ is equally insignificant. The fractional amount energy contained between $k_{min} = 10^{-5}$ and $k_{max} = 10^3$ is 99.3% for slab turbulence and 98.7% for 2D turbulence, indicating that the choice of minimum and maximum wave numbers is indeed very reasonable.

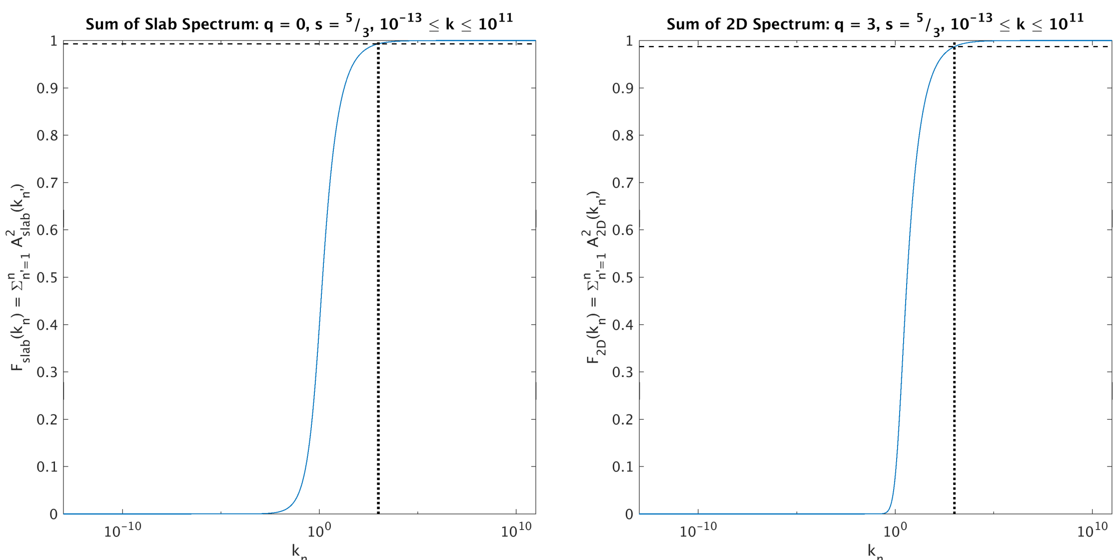

Figure 3.1: Normalized cumulative sum of the spectrum function $G(k_n, q+1, s-1)$, for Slab (right) and 2D (left) models. The dashed line shows the fraction of the total magnetic energy below $k_{max} = 10^3$, and the dotted line denotes the location of $k = 10^3$.

3.4 Particle Trajectory Solver

As stated in 3.9, our unitless equations of motion are given by

$$\frac{\mathrm{d}\vec{R}}{\mathrm{d}\tau} = \vec{R} \times \vec{b}(\vec{\chi}), \qquad \frac{\mathrm{d}\vec{\chi}}{\mathrm{d}\tau} = \vec{R}.$$

Since we also know that the magnitude of the rigidity must be conserved, we can use that as a requirement of the integration method we use. To that end, a modified third-order symplectic integration method is used to solve the particle trajectories. The reason for using a symplectic integration method instead of a Runge-Kutta method is that while neither will conserve the energy of the particle normally, the symplectic method is capable of being modified to achieve a much higher degree of conservation.

3.4.1 Third-Order Symplectic Integration Equations

The basic third-order symplectic method is written as follows (Yoshida, 1992):

$$\vec{p}_1 = \vec{p}(t) + P_1 \frac{\mathrm{d}\vec{p}}{\mathrm{d}t}(\vec{p}(t), \vec{q}(t))\mathrm{d}t, \qquad \vec{q}_1 = \vec{q}(t) + Q_1 \frac{\mathrm{d}\vec{q}}{\mathrm{d}t}(\vec{p}_1, \vec{q}(t))\mathrm{d}t,$$

$$\vec{p}_2 = \vec{p}_1 + P_2 \frac{\mathrm{d}\vec{p}}{\mathrm{d}t}(\vec{p}_1, \vec{q}_1)\mathrm{d}t, \qquad \vec{q}_2 = \vec{q}_1 + Q_2 \frac{\mathrm{d}\vec{q}}{\mathrm{d}t}(\vec{p}_2, \vec{q}_1)\mathrm{d}t,$$

$$\vec{p}(t+\mathrm{d}t) = \vec{p}_2 + P_3 \frac{\mathrm{d}\vec{p}}{\mathrm{d}t}(\vec{p}_2, \vec{q}_2)\mathrm{d}t, \qquad \vec{q}(t+\mathrm{d}t) = \vec{q}_2 + Q_3 \frac{\mathrm{d}\vec{q}}{\mathrm{d}t}(\vec{p}(t+\mathrm{d}t), \vec{q}_2)\mathrm{d}t.$$

Here, P_i and Q_i $(i = 1, 2, 3)$ are the integration coefficients for canonical momentum $\vec{p}$ and canonical position $\vec{q}$, respectively. The values of the coefficients are defined by several equations, two of which require $\sum Q_i = 1$ and $\sum P_i = 1$. Table 3.2 lists the values of the coefficients that were used in the the simulations. These equations are specifically designed to use Hamilton's equations to calculate $\frac{\mathrm{d}\vec{p}}{\mathrm{d}t}$ and $\frac{\mathrm{d}\vec{q}}{\mathrm{d}t}$, which in our case turns out to be a problem. The benefit of using these equations is that the final updated momentum and position do not require averaging over the intermediate steps.

The primary problem with using Hamilton's equations for unbound particles in a

	$i=1$	$i=2$	$i=3$
Q_i	$^2/_3$	$^{-2}/_3$	1
P_i	$^7/_{24}$	$^3/_4$	$^{-1}/_{24}$

Table 3.2: Table of symplectic integration coefficients

turbulent magnetic field is that the potential for the mean field becomes arbitrarily large as the particle moves away from the origin. While it is possible to solve this problem by changing the mean field potential to $\frac{1}{2}\hat{z} \times (\vec{\chi} - \vec{\chi}_c)$, with $\vec{\chi}_c$ being the particles guiding center, this increases the amount of time required to calculate the updated position and momentum. Furthermore, it remains dubious whether or not the energy of the particles would be conserved, as the two quantities that are coupled by the magnetic field are not position and momentum, but rather the two velocity vectors perpendicular to the magnetic field. Finally, we are not concerned with the canonical position and momentum, but with the position and velocity as they appear in the Lorentz force.

Replacing the canonical position, momentum, and associated derivatives with the unitless particle position, velocity, and Lorentz force yields the following:

$$\begin{aligned}
\vec{R}_1 &= \vec{R}(\tau) + P_1\vec{R}(\tau) \times \vec{b}(\vec{\chi}(\tau))\mathrm{d}\tau, & \vec{\chi}_1 &= \vec{\chi}(\tau) + Q_1\vec{R}_1\mathrm{d}\tau, \\
\vec{R}_2 &= \vec{R}_1 + P_2\vec{R}_1 \times \vec{b}(\vec{\chi}(\tau))\mathrm{d}\tau, & \vec{\chi}_2 &= \vec{\chi}_1 + Q_2\vec{R}_2\mathrm{d}\tau, \qquad (3.40) \\
\vec{R}(\tau + \mathrm{d}\tau) &= \vec{R}_2 + P_3\vec{R}_2 \times \vec{b}(\vec{\chi}(\tau))\mathrm{d}\tau, & \vec{\chi}(\tau + \mathrm{d}\tau) &= \vec{\chi}_2 + Q_3\vec{R}(\tau + \mathrm{d}\tau)\mathrm{d}\tau.
\end{aligned}$$

In the above equations we used the magnetic field at $\vec{\chi}(\tau)$ in each step, since recalculating the field each time approximately triples the amount of time it takes to run the simulation. For the purpose of analysis, we rewrite the cross product to get

$$\vec{R} \times \vec{b} = R_j b_k \epsilon_{ijk} = \bar{\bar{b}}_{ij} R_j = \bar{\bar{b}} \vec{R}. \tag{3.41}$$

In matrix form, $\bar{\bar{b}}_{ij} = \epsilon_{ijk} b_k$ can be written as

$$\bar{\bar{b}} = \begin{pmatrix} 0 & b_z & -b_y \\ -b_z & 0 & b_x \\ b_y & -b_x & 0 \end{pmatrix}, \tag{3.42}$$

which can be inserted into the velocity equations listed in, 3.41 to get

$$\vec{R}_1 = \bar{\bar{I}} \vec{R}(\tau) + P_1 \bar{\bar{b}}(\vec{\chi}(\tau)) \vec{R}(\tau) \mathrm{d}\tau, \tag{3.43a}$$

$$\vec{R}_2 = \bar{\bar{I}} \vec{R}_1 + P_2 \bar{\bar{b}}(\vec{\chi}(\tau)) \vec{R}_1 \mathrm{d}\tau, \tag{3.43b}$$

$$\vec{R}(\tau + \mathrm{d}\tau) = \bar{\bar{I}} \vec{R}_2 + P_3 \bar{\bar{b}}(\vec{\chi}(\tau)) \vec{R}_2 \mathrm{d}\tau, \tag{3.43c}$$

where $\bar{\bar{I}}$ is the identity matrix. This matrix has the property that $\bar{\bar{b}}^\dagger = -\bar{\bar{b}}$ and $\bar{\bar{b}}^2 = \vec{b}_i \vec{b}_j - \delta_{ij} |\vec{b}|^2$. For analysis purposes, we define a new quantity $\bar{\bar{\omega}} = \bar{\bar{b}} \mathrm{d}\tau$, and then rearrange the equations in 3.43 to get

$$\begin{aligned} \vec{R}_1 &= \left(\bar{\bar{I}} + P_1 \bar{\bar{\omega}}(\vec{\chi}(\tau)) \right) \vec{R}(\tau), \\ \vec{R}_2 &= \left(\bar{\bar{I}} + P_2 \bar{\bar{\omega}}(\vec{\chi}(\tau)) \right) \vec{R}_1, \\ \vec{R}(\tau + \mathrm{d}\tau) &= \left(\bar{\bar{I}} + P_3 \bar{\bar{\omega}}(\vec{\chi}(\tau)) \right) \vec{R}_2. \end{aligned} \tag{3.44}$$

Finally, we can combine the individual equations in 3.44 to get

$$\begin{aligned}\vec{R}(\tau + \mathrm{d}\tau) &= \left(\bar{\bar{I}} + P_1\bar{\bar{\omega}}(\vec{\chi}(\tau))\right)\left(\bar{\bar{I}} + P_2\bar{\bar{\omega}}(\vec{\chi}(\tau))\right)\left(\bar{\bar{I}} + P_3\bar{\bar{\omega}}(\vec{\chi}(\tau))\right)\vec{R}(\tau) \\ &= \left(\bar{\bar{I}} + \bar{\bar{\omega}} + (P_1P_2 + P_1P_3 + P_2P_3)\bar{\bar{\omega}}^2 + P_1P_2P_3\bar{\bar{\omega}}^3\right)\vec{R}(\tau). \qquad (3.45)\end{aligned}$$

3.4.2 Symplectic Integration Error Analysis

In a constant, uniform magnetic field, the particle's velocity would be calculated for all time by

$$\vec{R}(n\mathrm{d}\tau) = \left(\bar{\bar{I}} + \bar{\bar{\omega}} + (P_1P_2 + P_1P_3 + P_2P_3)\bar{\bar{\omega}}^2 + P_1P_2P_3\bar{\bar{\omega}}^3\right)^n \vec{R}_0. \qquad (3.46)$$

Substituting in the values of P_i, we get

$$\vec{R}(n\mathrm{d}\tau) = \left(\bar{\bar{I}} + \bar{\bar{\omega}} + \frac{101}{576}\bar{\bar{\omega}}^2 - \frac{21}{2304}\bar{\bar{\omega}}^3\right)^n \vec{R}_0. \qquad (3.47)$$

The fractional change in the particle energy to second order can be found by

$$\begin{aligned}\frac{|\vec{R}|^2(\mathrm{d}\tau)}{|\vec{R}_0|^2} &= \frac{\vec{R}^\dagger(n\mathrm{d}\tau)\cdot\vec{R}(n\mathrm{d}\tau)}{R_0^2} \\ &= \frac{\vec{R}_0\left(\bar{\bar{I}} - \bar{\bar{\omega}} + \frac{101}{576}\bar{\bar{\omega}}^2 + \frac{21}{2304}\bar{\bar{\omega}}^3\right)\left(\bar{\bar{I}} + \bar{\bar{\omega}} + \frac{101}{576}\bar{\bar{\omega}}^2 - \frac{21}{2304}\bar{\bar{\omega}}^3\right)\vec{R}_0}{R_0^2} \\ &= \frac{\vec{R}_0\left(\bar{\bar{I}} - (1 - \frac{101}{288})\bar{\bar{\omega}}^2 + \cdots\right)\vec{R}_0}{R_0^2} \\ &= \frac{\vec{R}_0^2 - (1 - \frac{101}{288})\vec{R}_0\bar{\bar{\omega}}^2\vec{R}_0}{R_0^2} \\ &= 1 + \frac{187}{288}(|\vec{b}|\mathrm{d}\tau)^2\sin^2(\theta). \qquad (3.48)\end{aligned}$$

In the above equation, we used a cross product identity to convert $-\vec{R}_0\bar{\bar{\omega}}^2\vec{R}_0$ to $R_0^2|\vec{b}|^2\mathrm{d}\tau\sin^2(\theta)$, where θ is the angle between the magnetic field and the velocity vector. The total change in energy after a given amount of time is calculated as

$$\frac{|\vec{R}|^2(n\mathrm{d}\tau)}{|\vec{R}_0|^2} = \left(1 + \frac{187}{288}(|\vec{b}|\mathrm{d}\tau)^2\sin^2(\theta)\right)^n, \tag{3.49}$$

meaning that the particle continually gains energy based on the relative orientation of its velocity to the magnetic field.

3.4.3 Modified Symplectic Integration Method

In order to achieve greater energy conservation, I modified the symplectic method by taking advantage of the fact that action of a uniform magnetic field on a particle trajectory causes the velocity perpendicular to the field to rotate around the field with a frequency proportional to $|\vec{b}|$. We begin by defining a coordinate rotation matrix $\bar{\bar{M}}$, such that

$$\bar{\bar{M}}\hat{b} = \begin{pmatrix} 1 \\ 0 \\ 0 \end{pmatrix}. \tag{3.50}$$

The velocity vector in the new coordinate system is then given by

$$\vec{R}' = \bar{\bar{M}}\vec{R} = \begin{pmatrix} \vec{R}_r \\ \vec{R}_\theta \\ \vec{R}_\phi \end{pmatrix}. \tag{3.51}$$

In this new coordinate system, the exact solution to the velocity equation for a uniform field is given by

$$\vec{R}'(\tau + \mathrm{d}\tau) = \bar{\bar{F}}'(|\vec{b}|\mathrm{d}\tau)\vec{R}'(\tau), \tag{3.52}$$

where matrix $\bar{\bar{F}}'(x)$ is equal to

$$\bar{\bar{F}}'(x) = \begin{pmatrix} 1 & 0 & 0 \\ 0 & \cos(x) & \sin(x) \\ 0 & -\sin(x) & \cos(x) \end{pmatrix}. \tag{3.53}$$

This implies that the solution in the non-rotated reference frame is found by

$$\vec{R}(\tau + \mathrm{d}\tau) = \bar{\bar{M}}^{\dagger}\bar{\bar{F}}'(|\vec{b}|\mathrm{d}\tau)\bar{\bar{M}}\vec{R}(\tau) = \bar{\bar{F}}(|\vec{b}|\mathrm{d}\tau)\vec{R}(\tau). \tag{3.54}$$

Since $\bar{\bar{F}}$ is a unitary rotation matrix, the change in the particle energy can be written as

$$\frac{R^2(\tau)}{R_0^2} = (1+\epsilon)^{\frac{\tau}{\mathrm{d}\tau}}, \tag{3.55}$$

where ϵ is the numerical error on $\bar{\bar{F}}^{\dagger}\bar{\bar{F}} = \bar{\bar{I}}$.

Substituting equation 3.54 into the equations in 3.44 and 3.40 yields the set of equations we use for solving the particle trajectories:

$$\begin{aligned} \vec{R}_1 &= \bar{\bar{F}}\Big(P_1 b\big(\vec{\chi}(\tau)\big)\mathrm{d}\tau\Big)\vec{R}(\tau) & \vec{\chi}_1 &= \vec{\chi}(\tau) + Q_1\vec{R}_1\mathrm{d}\tau, \\ \vec{R}_2 &= \bar{\bar{F}}\Big(P_2 b\big(\vec{\chi}(\tau)\big)\mathrm{d}\tau\Big)\vec{R}_1, & \vec{\chi}_2 &= \vec{\chi}_1 + Q_2\vec{R}_2\mathrm{d}\tau, \\ \vec{R}(\tau+\mathrm{d}\tau) &= \bar{\bar{F}}\Big(P_3 b\big(\vec{\chi}(\tau)\big)\mathrm{d}\tau\Big)\vec{R}_2, & \vec{\chi}(\tau+\mathrm{d}\tau) &= \vec{\chi}_2 + Q_3\vec{R}(\tau+\mathrm{d}\tau)\mathrm{d}\tau. \end{aligned} \tag{3.56}$$

The result of using these equations is that at each time step the velocity vector is rotated by a small angle around the magnetic field at the point the particle occupies, and the rotation becomes exact as $\mathrm{d}\tau$ approaches zero. In the general case, the solution can be considered to be exact in terms of velocity as long as the magnetic field does not vary by any significant amount between $\vec{\chi}(\tau)$ and $\vec{\chi}(\tau + \mathrm{d}\tau)$, and the condition that $b\big(\vec{\chi}(\tau)\big)\mathrm{d}\tau \ll 1$ is satisfied. Figure 3.2 shows the comparison in energy conservation between a non-adaptive RK4 method and the modified symplectic method used for various magnetic field strengths. Additional testing with $\mathrm{d}\tau = 10^{-3}$ indicates that for field magnitudes greater than π, the modified symplectic method results in better energy conservation, while for lower field magnitudes the RK4 method provides better conservation. This is important as the magnitude of the magnetic field will vary from point to point, and the modified symplectic method has an error that is smaller for larger field magnitudes.

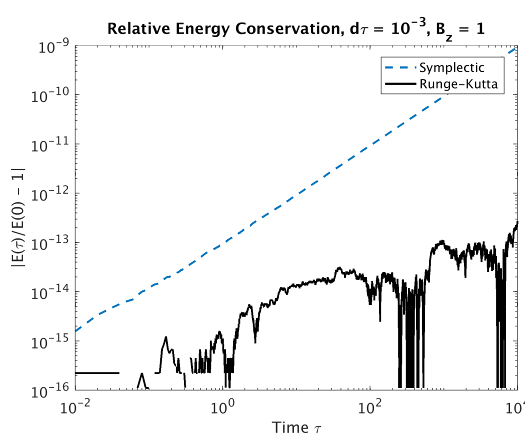

(a) $\vec{B} = (0, 0, 1)$

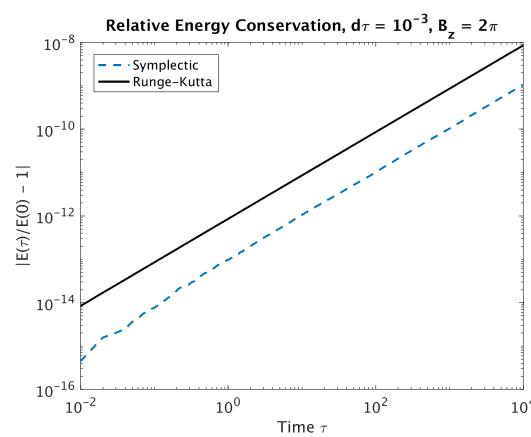

(b) $\vec{B} = (0, 0, 2\pi)$

Figure 3.2: Relative energy conservation for an RK4 method and the modified symplectic integrator

3.5 Particle Trajectory Simulation Method

In each simulation the problem of solving the particle trajectories is broken up into smaller subsystems to allow for the overall problem to be run in parallel, decreasing the amount of time it takes to generate a set of trajectories. Each subsystem has its own magnetic field realization: the model is the same, but the orientation of the wave vectors, field vectors, and phase offsets are randomized within the parameters of that model; in general no two field realizations are exactly the same. This is equivalent to choosing different field realizations at random from the ensemble used to derive the magnetic correlation tensor and models. During the simulation, the particle parameters are kept at set intervals, rather than at every point in time. This reduces both the memory and storage space requirements for each simulation, and the amount of time required to analyze the resulting trajectories. This means that the time step between points that are kept is given by $\mathrm{d}\tau' = T_{steps}\mathrm{d}\tau$, where T_{steps} is the number of time steps between outputs. In general the value of T_{steps} was between $\mathrm{d}\tau^{-1}$ and $10\mathrm{d}\tau^{-1}$, such that $\mathrm{d}\tau'$ was an integer.

After a set of particle trajectories have been obtained, analysis is performed to obtain several quantities of interest for this thesis. Specifically, we are interested in the diffusion coefficients for the particles, the particle displacement densities, the characteristic function for the system, and the velocity correlations. Calculating each of these quantities involves averaging over all trajectories, regardless of the specific individual field realizations. Since the particles are given random initial starting positions, we use the particle displacement $\Delta\vec{\chi} = \vec{\chi}(\tau) - \vec{\chi}(\tau = 0)$ instead of the particle positions during analysis.

Chapter 4

Computational Analysis

The indexing convention used throughout this chapter is based on the methods used in the simulation and analysis code. The conventions are as follows:

- The overall simulation is spread across multiple CPU cores, each core having a different realization of the field. Therefore, there are F field realizations, with indexes denoted by a subscript f.

- Every field realization has the same number of particles in it, given by P_f. The total number of particles across the entire simulation is therefore given by $P = FP_f$. Individual particle indexes are given by a subscript p if referring to the total number of particles, or a subscript p_f if referring to particles in a specific realization.

- The simulation tracks the particle trajectories from $\tau = 0$ to $\tau = \tau_{max}$. Unlike the field realization or particle indexes, the index for points in time runs from zero to N, with $\tau_0 = 0$ and $\tau_N = \tau_{max}$. The points in time at which the particle trajectory is stored are denoted τ_n and the spacing between the points in time is given by $\mathrm{d}\tau'$.

4.1 Diffusion Coefficient Calculation

When calculating the diffusion coefficient, κ_{ii}, we use three different definitions: a late time approximation, the position velocity correlation, and a numerical time derivative. The results can then be compared to each other for agreement.

4.1.1 Late Time Approximation

The late time approximation (LTA) diffusion coefficient, κ_{ii}^{LTA}, comes from equation 2.3a. In terms of the individual particle trajectories this can be written as

$$\kappa_{ii}(\tau_n) = \frac{1}{2\tau_n}\frac{1}{P}\sum_{p=1}^{P}\left(\Delta\chi_{p,i}(\tau_n)\right)^2. \tag{4.1}$$

This method is generally valid only after the particle motion has become diffusive after a sufficiently long period of time. Conversely, the results from this method are easier to interpret as they do not vary much in time on small time scales.

4.1.2 Position Velocity Correlation

The position velocity correlation (PVC), κ_{ii}^{PVC}, and numerical time derivative (NTD), κ_{ii}^{NTD}, definitions are derived from equation 2.3b. The PVC definition can be calculated by bringing the time derivative inside the ensemble average, and then taking the derivative analytically, yielding

$$\kappa_{ii}(\tau) = \langle\Delta\chi_i(\tau)R_i(\tau)\rangle. \tag{4.2}$$

In terms of individual particle trajectories, this can be written as

$$\kappa_{ii}(\tau_n) = \frac{1}{P}\sum_{p=1}^{P} \Delta\chi_{p,i}(\tau_n) R_{p,i}(\tau_n). \tag{4.3}$$

This method has more variance between points in time than the late time approximation and therefore requires an increase in the number of particle trajectories when determining if a model results in diffusion. However, it can provide insight into the behavior of the diffusion coefficient when the first method gives a non-diffusive result.

4.1.3 Numerical Time Derivative

The final definition for the diffusion coefficient, κ_{ii}^{NTD}, uses the same procedure as the PVC definition, except the derivative is taken numerically instead of analytically. The equation for the diffusion coefficient is then

$$\kappa_{ii}(\tau_n) = \frac{\langle(\Delta\chi_i(\tau_n))^2 - (\Delta\chi_i(\tau_{n-1}))^2\rangle}{2(\tau_n - \tau_{n-1})} = \frac{\langle(\Delta\chi_i(\tau_n))^2 - (\Delta\chi_i(\tau_{n-1}))^2\rangle}{2\mathrm{d}\tau'}. \tag{4.4}$$

This method has similar advantages and drawbacks compared to the PVC definition, it has more variance in time but can give insight when the late time diffusion coefficient is non-diffusive. In terms of the individual particle trajectories, this definition for the diffusion coefficient is calculated as

$$\kappa_{ii}(\tau_n) = \frac{1}{2\mathrm{d}\tau'}\frac{1}{P}\sum_{p=1}^{P}\left(\big(\Delta\chi_{p,i}(\tau_n)\big)^2 - \big(\Delta\chi_{p,i}(\tau_{n-1})\big)^2\right). \tag{4.5}$$

4.1.4 Calculating the Diffusion Coefficients

For each of the methods for obtaining a diffusion coefficient, the simulation calculates the diffusion coefficient for each field realization. Then the results are averaged together during analysis to get a final coefficient. This can be written as

$$\kappa_{ii} = \frac{1}{F} \sum_{f=1}^{F} \kappa_{ii,f}, \tag{4.6}$$

with $\kappa_{ii,f}$ being the diffusion coefficient for field realization f. Since the turbulence models used are axisymmetric, we can reduce the diffusion coefficient to parallel and perpendicular coefficients given by equations 2.21 and 2.23

4.1.5 Comparison of Different Definitions

During analysis, the diffusion coefficients are calculated for each of the above definitions, which are then compared to each other. In general, the position velocity correlation method results in the most variance in time, even when the result fluctuates around a constant. However, the numerical time derivative definition can be related to the late time approximation by

$$\kappa_{ii}^{LTA}(\tau_n) = \frac{1}{\tau_n} \sum_{n'=1}^{n} \kappa_{ii}^{NTD}(\tau_{n'}) \mathrm{d}\tau' = \frac{1}{n} \sum_{n'=1}^{n} \kappa_{ii}^{NTD}(\tau_{n'}). \tag{4.7}$$

Similarly, we can relate the PVC method to the late time approximation by

$$\kappa_{ii}^{LTA}(\tau) = \frac{1}{\tau} \int_{0}^{\tau} \kappa_{ii}^{PVC}(\tau') \mathrm{d}\tau'. \tag{4.8}$$

From the above equations, we can state that the late time approximation is equivalent to a time average of the derivative based definitions.

4.2 Particle Density

The particle density is calculated by projecting the displacement of each particle at specific times along the x, y, and z axes; and then creating a histogram for each of the resulting projections. Once the densities have been calculated, the results are refined so that bins at the edge contain approximately 0.1% of the total particle density. Finally, given the theoretical assumption that the particle distribution will take the form of a Gaussian, we overlay a normalized Gaussian distribution centered at zero, with a value of σ given by

$$\sigma_i(\tau_n) = \sqrt{2\tau_n \kappa_{ii}^{LTA}(\tau_n)} = \left\langle (\Delta\chi_i(\tau_n))^2 \right\rangle^{\frac{1}{2}}. \tag{4.9}$$

4.3 Characteristic Function

As defined in equation 2.18, the characteristic function is given by

$$\tilde{\rho}(\vec{k}, \tau) = \left\langle e^{i\vec{k}\Delta\vec{x}} \right\rangle. \tag{4.10}$$

When calculating this quantity numerically we use spherical coordinates, and then take slices along the z axis or in the $k_\theta = \pi/2$ plane for slab or 2D turbulence respectively, and both projections are taken for composition. Since we are using spherical coordinates, the function is calculated one particle at a time rather than with a FFT algorithm. This method avoids artifacts that would arise from binning the particle trajectories and allows for manual control over the resolution in wavenumber. The significant drawback comes from the lack of speed in calculation: the average amount of time to calculate the characteristic function and velocity correlation is around five hours for the number of particles used in the simulations.

Instead of using the wave vectors from the actual simulation, we divide $0 \leq k_\theta \leq \pi$ into 21 equally spaced points and $0 \leq k_\phi < 2\pi$ into 20 equally spaced points, for a total of 420 different unit vectors. The wave number is then divided into 1000 equally spaced points using $0 < k_r \leq k_{max}$, where k_{max} is set manually before each simulation is run and is separate from the maximum wave number used to generate the turbulence. Since the maximum wave number is set manually, the analysis can be rerun without having to run an entirely new simulation if the maximum wavelength is too large or not large enough to properly capture the characteristic function. Calculating this quantity numerically can therefore be written as

$$\tilde{\rho}(\vec{k}, \tau) = \frac{1}{P} \sum_{p=1}^{P} \int_{\mathbb{V}} \delta(\Delta\vec{\chi} - \Delta\vec{\chi}_p(\tau)) e^{i\vec{k}\Delta\vec{\chi}} \mathrm{d}^3\chi = \frac{1}{P} \sum_{p=1}^{P} e^{i\vec{k}\Delta\vec{\chi}_p(\tau)}, \tag{4.11}$$

since the individual particles have a density given by a delta function. The projection into the z axis or $k_\theta = \pi/2$ plane is then done by averaging over k_ϕ; for the z axis projection this is equivalent to randomly selecting one of the values of k_ϕ for use, while for the $k_\theta = \pi/2$ plane projection the averaging removes any fluctuations in k_ϕ. The final result is a function of one spatial coordinate and time.

4.4 Velocity Correlation

The purpose of calculating both the exact and approximate fourth order velocity correlations is to test the validity of the approximation in equation 2.42 and the assumption stated in equation 2.43. The unitless version of the equation 2.42 is

$$\left\langle R_z(0)R_z(\tau)e^{ik\Delta\vec{\chi}(\tau)}\right\rangle = \left\langle R_z(0)R_z(\tau)\right\rangle\left\langle e^{ik\Delta\vec{\chi}(\tau)}\right\rangle. \tag{4.12}$$

Besides the characteristic function, we refer to the quantities as the exact fourth order velocity correlation $EVC(\vec{k},\tau) = \left\langle R_z(0)R_z(\tau)e^{ik\Delta\vec{\chi}(\tau)}\right\rangle$, and the second order velocity correlation $V_{corr}(\tau) = \langle R_z(0)R_z(\tau)\rangle$. During analysis, these quantities are calculated by

$$EVC(\vec{k},\tau_n) = \frac{1}{P}\sum_{p=1}^{P} R_{z,p}(0)R_{z,p}(\tau_n)e^{i\vec{k}\Delta\vec{\chi}_p(\tau_n)}, \tag{4.13}$$

$$V_{corr}(\tau_n) = \frac{1}{P}\sum_{p=1}^{P} R_{z,p}(0)R_{z,p}(\tau_n). \tag{4.14}$$

The exact fourth order velocity correlation is calculated at the same time as the characteristic function in order to reduce the amount of time required for analysis, while the second order velocity correlation is calculated separately. For analysis, the exact fourth order velocity correlation is qualitatively compared to its approximation, and the second order velocity correlation is compared to its assumed form by overlaying the calculated form with equation 2.43.

Chapter 5

Results

The results presented in this chapter use the same models that were used in generating the data sets for Arendt and Shalchi (2018). However, several changes to the non-model parameters were made to increase the statistical particle counts, and as a result the data sets used for Arendt and Shalchi (2018) are not incorporated into this thesis. Table 5.1 lists the common parameters and their values in Arendt and Shalchi (2018) and in this thesis. For general turbulence parameters, refer back to table 3.1.

Parameter	Arendt and Shalchi (2018)	*Thesis*
Number of Field Realizations	120	960
Number of Particles per Field	100	75
Total Number of Particles	12000	72000
Time Step Size, $\mathrm{d}\tau$	10^{-3}	10^{-3}
Time Between Outputs, $\mathrm{d}\tau'$	1	5
Maximum Time, τ_{max}	5000	10000

Table 5.1: List of parameters not specific to the magnetic turbulence models.

As mentioned in 2.3, there are several parameters that can be varied when creating composite turbulence. In this thesis we used four parameter sets for composite turbulence, denoted as models 1 through 4. The first set used equal length scales and had 20% of its energy contained in the slab component and 80% in the 2D component. The total turbulent energy in this model is equal to the energy of the mean field. The second set has the same energy distribution and total energy of the first model, but uses a 2D length scale ratio of $\ell = 0.1$. The third set uses the same energy distribution and length scales as the first model, but lowers the total turbulent energy to one quarter of the mean field. The final set keeps the total energy and length scale of the third model, but changes the energy distribution to 80% slab and 20% 2D. Table 5.2 summarizes each of the models used, as well as the rigidities that we simulated in each model.

Model Name	db^2_{Total}	db^2_{Slab}	db^2_{2D}	$^{l_{2D}}/_{l_{Slab}}$	*Simulated Rigidities*
Slab Model	1	1	0	N/A	$0.1, 1.0, 10.0$
2D Model	1	0	1	N/A	$0.1, 1.0$
Composite Model 1	1	0.2	0.8	1.0	$0.1, 1.0, 10.0$
Composite Model 2	1	0.2	0.8	0.1	$0.1, 1.0, 10.0$
Composite Model 3	0.25	0.2	0.8	1.0	$0.1, 1.0$
Composite Model 4	0.25	0.8	0.2	1.0	$0.1, 1.0$

Table 5.2: Table of parameters that define each unique model used.

5.1 Results for Pure Slab Turbulence

We performed simulations for three different rigidities, $R = 0.1$, $R = 1.0$, and $R = 10.0$, using the slab turbulence model. From a qualitative standpoint, the general behaviour of the various quantities is found to be independent of the particle rigidity, even though the exact values of the quantities change with rigidity. A comparison of the PVC and NTD definitions reveals that the numerical derivative definition has lower temporal fluctuations in value, as demonstrated in figure 5.1. The perpendicular

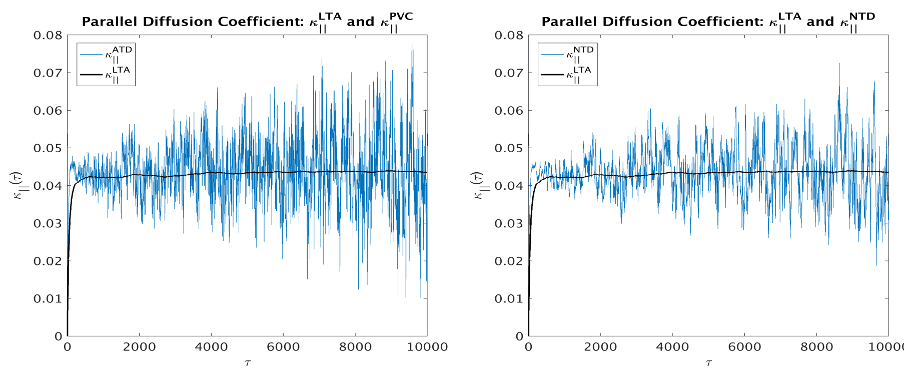

(a) Parallel diffusion coefficient

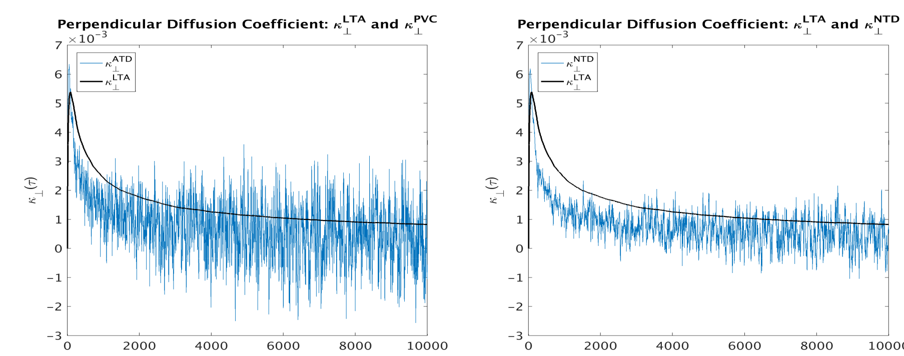

(b) Perpendicular diffusion coefficient

Figure 5.1: Diffusion coefficients for particles with a rigidity of $R = 0.1$ in slab turbulence.

diffusion coefficient $\kappa_{\perp}$ has a characteristic spike in early times before decaying. In particular $\kappa_{\perp}^{LTA}$ is sub-diffusive by the end of the simulations, however given the relations between the various diffusive coefficients in equations 4.7 and 4.8 and the amount of noise in the derivative definitions, it is difficult to say whether or not $\kappa_{\perp}^{LTA}$ is fully sub-diffusive with $\lim_{\tau \to \infty} \kappa_{\perp} = 0$, or if it will become diffusive at some future point. From previous work (Webb et al., 2006), we can conclude that $\kappa_{\perp}^{LTA}$ will remain sub-diffusive due to compound diffusion in reduced dimensional models such as the slab model. The parallel diffusion coefficient, on the other hand, shows a diffusive behaviour with minor fluctuations in $\kappa_{\parallel}^{LTA}$. Figure 5.2 shows the diffusion coefficients for rigidities $R = 1.0$ and $R = 10.0$, demonstrating that the behaviour of the the diffusion coefficients is similar for different rigidities.

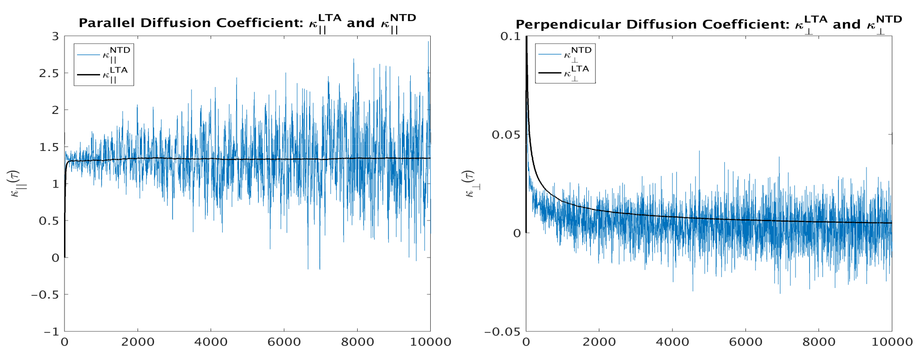

(a) Rigidity $R = 1.0$

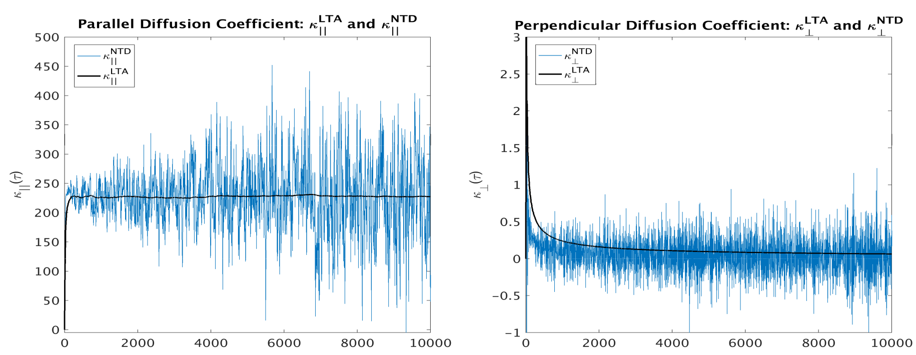

(b) Rigidity $R = 10.0$

Figure 5.2: Diffusion coefficients for particles with a rigidity of $R = 1.0$ (*top*) and $R = 10.0$ (*bottom*) in slab turbulence. The left column shows $\kappa_{\parallel}$, while the right column shows $\kappa_{\perp}$.

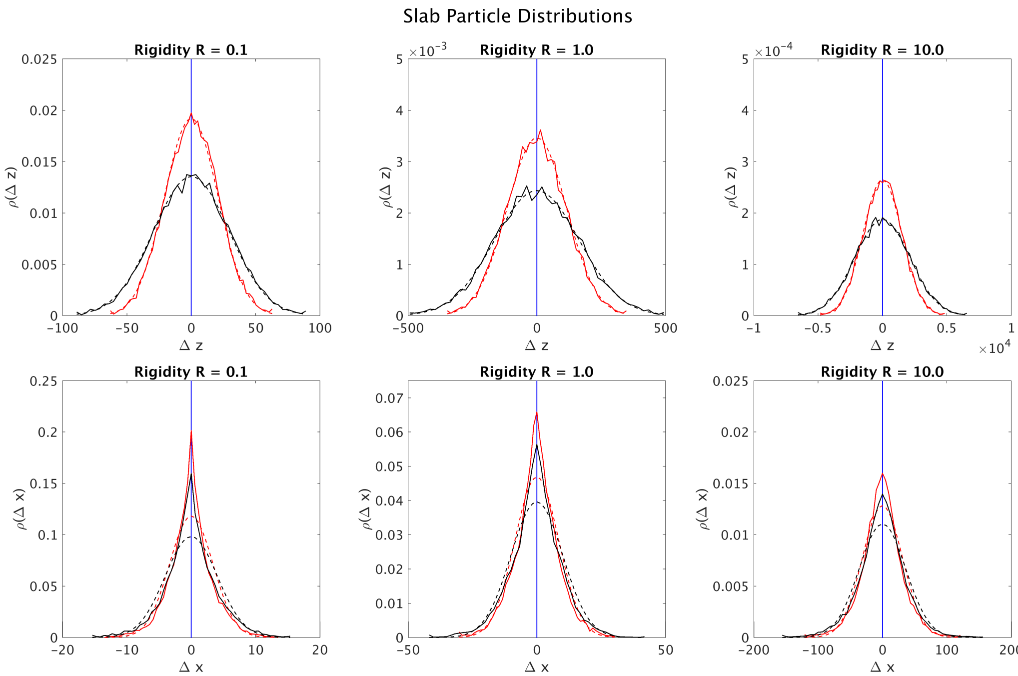

Figure 5.3: Particle distributions for slab turbulence. The dashed lines show the Gaussian distribution that results from the value of σ as calculated by equation 4.9. The times in each distribution are $\tau = 0$ (blue), $\tau = 5000$ (red), and $\tau = 10000$ (black). *Left Column*: $R = 0.1$; *Middle Column*: $R = 1.0$; *Right Column*: $R = 10.0$. *Top Row*: Distribution in Δz; *Bottom Row*: Distribution in Δx.

The particle distributions shown in figure 5.3 can be divided into two distinct distributions. The distribution as projected along the z axis can be well described by a Gaussian, while the distribution along the x axis is better described by the distributions in Webb et al. (2006) due to the sharp peak at zero. Given the nature of a Gaussian distribution under Fourier transform, we should expect that the characteristic function is also a Gaussian. In figure 5.4 we see that this is not the case, the characteristic functions all have an additional oscillatory pattern outside the main peak. This discrepancy can be attributed to two sources: first, the distribution functions were calculated at later times than those used for the characteristic function. The second is that for the times when the characteristic function is calculated, the particles are not yet diffusive along the z axis.

The second order parallal velocity correlation (figure 5.5) does show agreement between the calculated values and equation 2.43. However, the product of the second order correlation and the characteristic function is not a good approximation to the exact fourth order velocity correlation function (equation 2.42) as shown in figure 5.6. The exact fourth order correlation still has distinct oscillations as a function of wavenumber, while the temporal dependence has a slower decay rate then the normal velocity correlation.

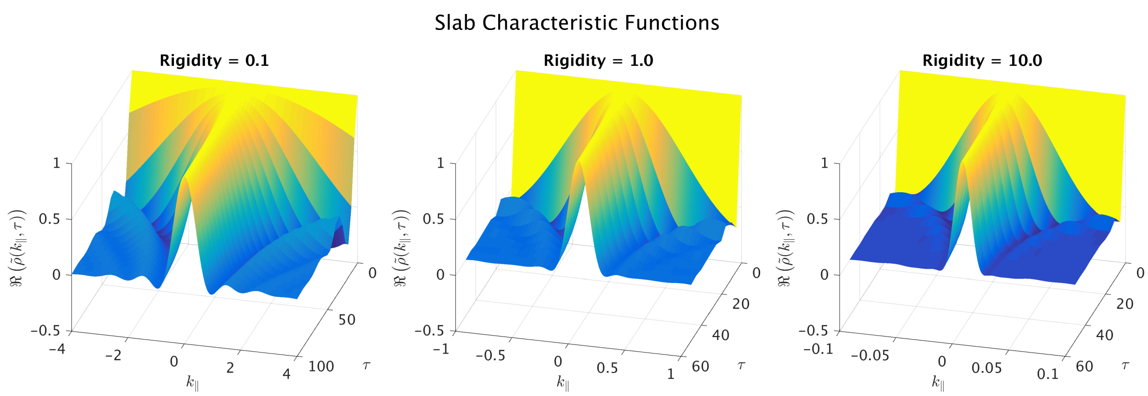

Figure 5.4: Real component of the characteristic function $\tilde{\rho}(k_\parallel, \tau)$ for slab turbulence. *Left*: $R = 0.1$; *Center*: $R = 1.0$; *Right*: $R = 10.0$

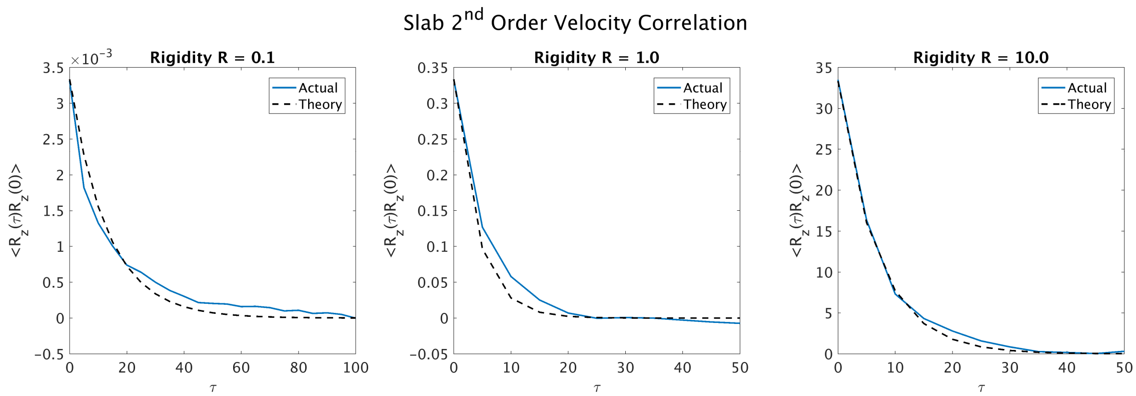

Figure 5.5: Second order velocity correlation (equation 2.43) for slab turbulence. The dashed line indicates the value of equation 2.43. *Left*: $R = 0.1$; *Center*: $R = 1.0$; *Right*: $R = 10.0$.

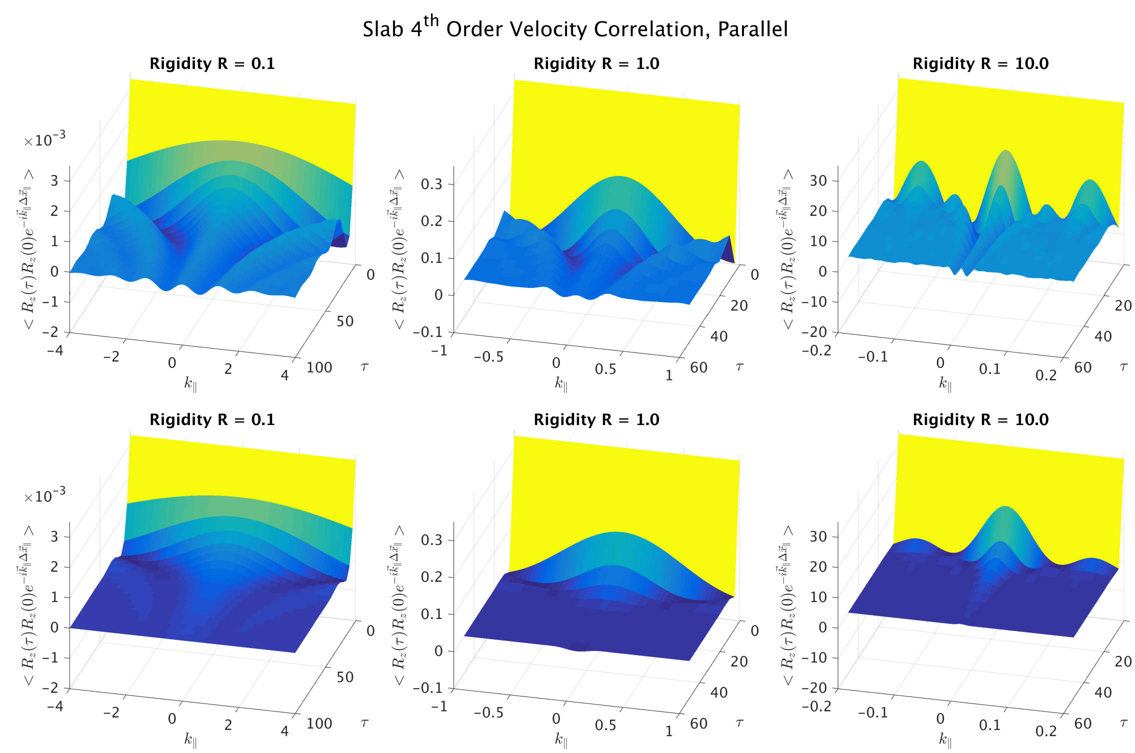

Figure 5.6: Comparison of the approximate and exact fourth order velocity correlation function for slab turbulence. *Left Column*: $R = 0.1$; *Middle Column*: $R = 1.0$; *Right Column*: $R = 10.0$. *Top Row*: Exact Correlation; *Bottom Row*: Approximate Correlation.

5.2 Result for Pure 2D Turbulence

Simulations for two dimensional turbulence were performed with particle rigidities of $R = 0.1$ and $R = 1.0$. As with the slab model results, the fluctuations in κ^{NTD} are lower than those in κ^{ATD}. Figure 5.7 shows the diffusion coefficients, and reveals large differences between κ^{NTD} and κ^{LTA}. For a rigidity of $R = 0.1$, $\kappa_{\parallel}^{LTA}$ is super-diffusive

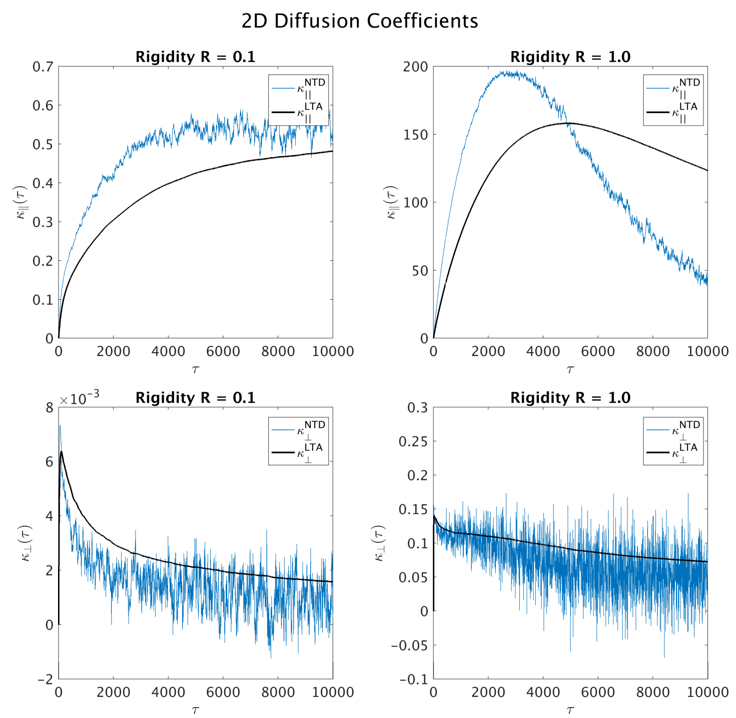

Figure 5.7: Diffusion coefficients for 2D turbulence. *Right Column*: $R = 0.1$; *Left Column*: $R = 1.0$; *Top Row*: Parallel Diffusion Coefficients; *Bottom Row*: Perpendicular Diffusion Coefficients.

and $\kappa_{\perp}^{LTA}$ is sub-diffusive. Looking at κ^{NTD}, however, shows that neither of the LTA diffusion coefficients have reached any final value (by equation 4.7) and the results are inconclusive as to the behaviour of $\kappa_{\perp}$ and $\kappa_{\parallel}$ as $\tau \to \infty$. At a rigidity of $R = 1.0$, we can see an even larger difference in the parallel diffusion coefficient, as both $\kappa_{\parallel}^{LTA}$ and $\kappa_{\parallel}^{NTD}$ begin super-diffusive and then transition to sub-diffusion. The perpendicular diffusion coefficient, however, shows sub-diffusive behaviour for the entire duration outside of the initial spike. With these results being incomplete in terms of temporal behaviour, it is no surprise that the second order velocity correlations (figure 5.8) do not match the theoretical assumptions. What is surprising however, is that the correlations do not appear to decay to zero.

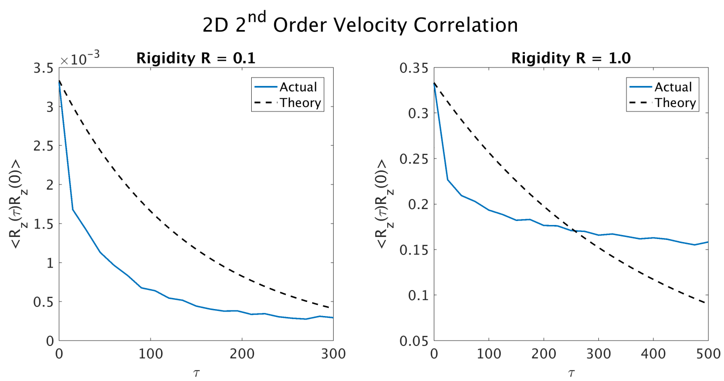

Figure 5.8: Second order velocity correlation (equation 2.43) for 2D turbulence. The dashed line indicates the value of equation 2.43. *Left*: $R = 0.1$; *Right*: $R = 1.0$.

Figure 5.9 shows the particle displacement distributions for the 2D model. The distribution functions for $R = 0.1$ do not resemble a Gaussian, and while the distributions for $R = 1.0$ come close, the distribution for Δz is lower at the peak, and the distribution for Δx is higher at the peak than the overlaid Gaussian function. As a result of this the characteristic functions in figure 5.10 are also non-Gaussian, but instead have a slow decay to zero at longer wave numbers. Figure 5.11 shows the result for the exact (*top*) and approximate (*bottom*) full velocity correlations. The exact correlation for $R = 0.1$ has a more well defined "edge" where the function transitions to an almost flat non-zero value compared to the approximation, which decays to zero. Beyond this, it is not possible to draw any more qualitative conclusions from the graphs.

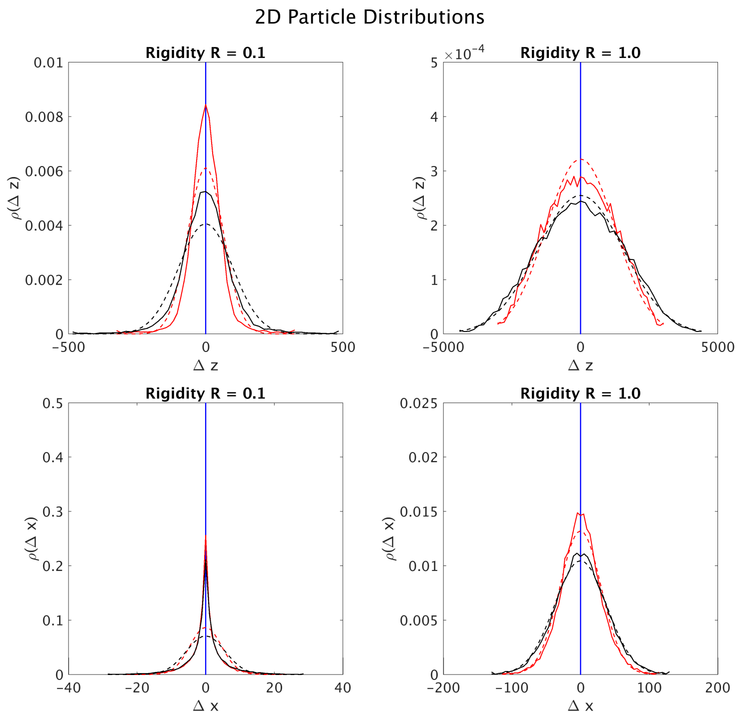

Figure 5.9: Particle distributions for 2D turbulence. The dashed lines are show the Gaussian distribution that results from the value of σ as calculated by equation 4.9. The times in each distribution are $\tau = 0$ (blue), $\tau = 5000$ (red), and $\tau = 10000$ (black). *Left Column*: $R = 0.1$; *Right Column*: $R = 1.0$. *Top Row*: Distribution in Δz; *Bottom Row*: Distribution in Δx.

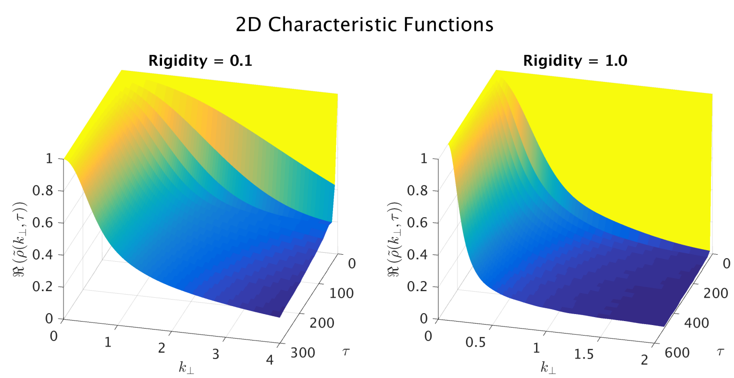

Figure 5.10: Real component of the characteristic function $\tilde{\rho}(k_\perp, \tau)$ for 2D turbulence. *Left*: $R = 0.1$; *Right*: $R = 1.0$

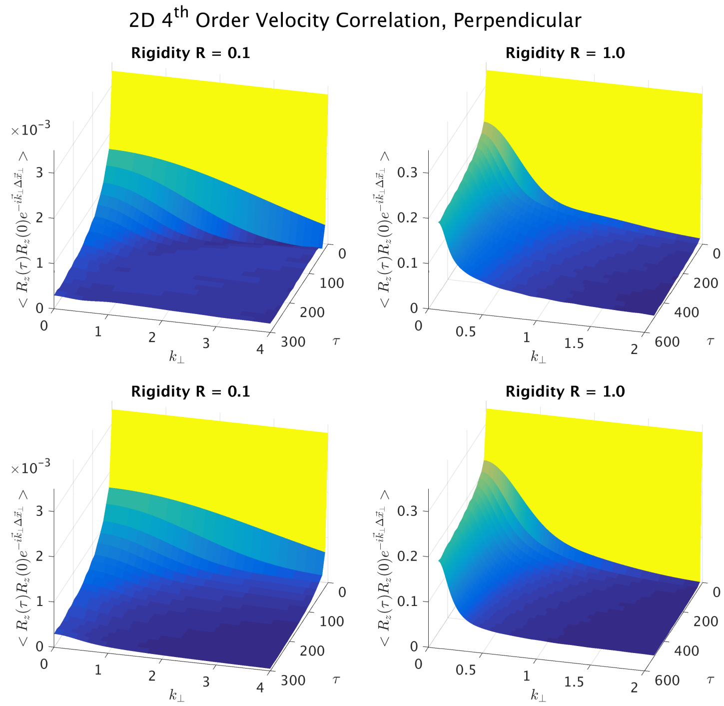

Figure 5.11: Comparison of the approximate and exact fourth order velocity correlation function for 2D turbulence. *Left Column*: $R = 0.1$; *Right Column*: $R = 1.0$. *Top Row*: Exact Correlation; *Bottom Row*: Approximate Correlation.

5.3 Results for Composite Turbulence: Model 1

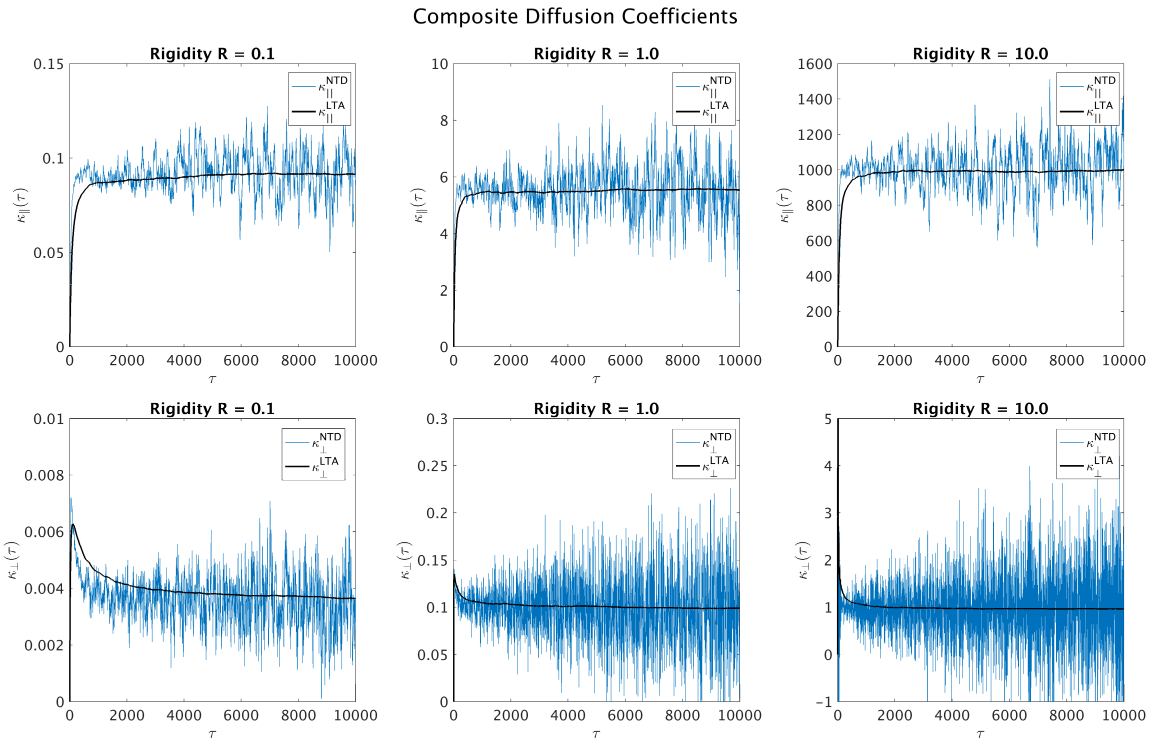

Figure 5.12: Diffusion coefficients for composite turbulence, model 1. *Right Column*: $R = 0.1$; *Middle Column*: $R = 1.0$ *Left Column*: $R = 10.0$; *Top Row*: Parallel Diffusion Coefficients; *Bottom Row*: Perpendicular Diffusion Coefficients.

Compared to the pure 2D turbulence, the parallel diffusion coefficients for the first composite model are indeed diffusive within the simulation time, although diffusion is not achieved as quickly as in the pure slab model. The perpendicular diffusion coefficients, however, appear to depend on the rigidity in terms of whether or not diffusive behaviour is reach. The particles with a rigidity of $R = 10.0$ achieve perpendicular diffusion, while the particles with $R = 0.1$ are still sub-diffusive. On close inspection of $\kappa_{\perp}^{LTA}$ for $R = 1.0$ we see very minor sub diffusive behaviour. However, when comparing $\kappa_{\perp}^{LTA}$ to $\kappa_{\perp}^{NTD}$, it is safe to say that because the fluctuations in $\kappa_{\perp}^{NTD}$ are not centered on zero, $\kappa_{\perp}^{LTA}$ will become diffusive at some point.

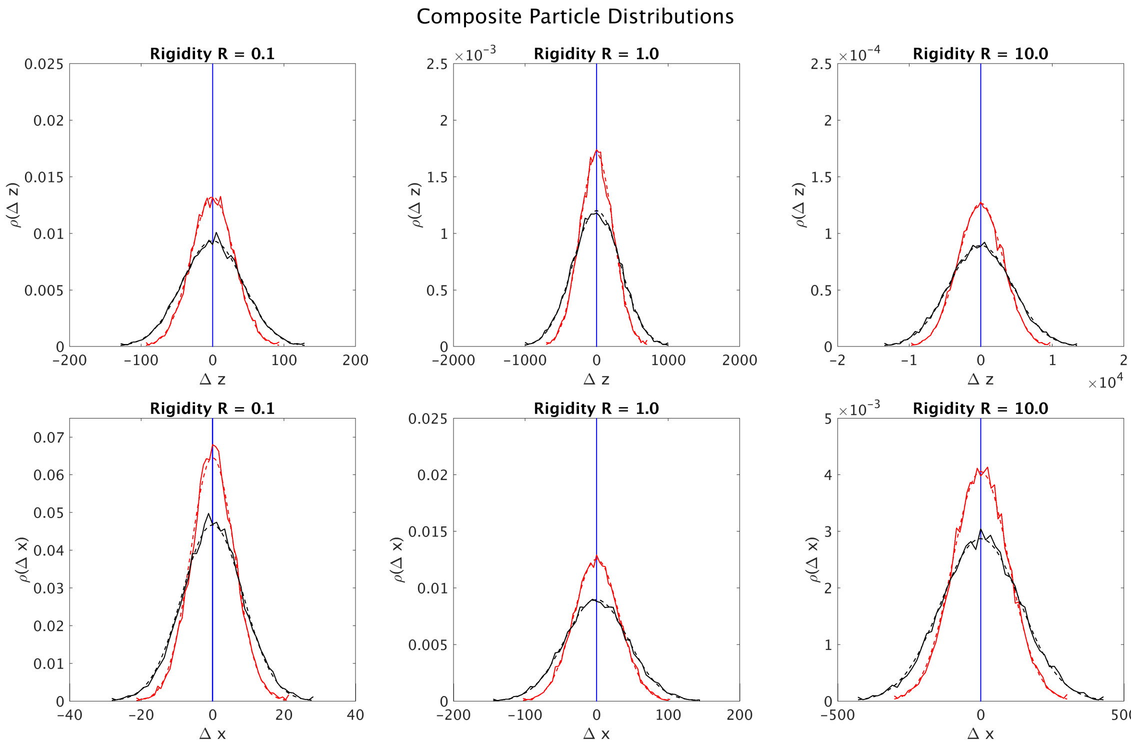

Figure 5.13: Particle distributions for composite turbulence, model 1. The dashed lines show the Gaussian distribution that results from the value of σ as calculated by equation 4.9. The times in each distribution are $\tau = 0$ (blue), $\tau = 5000$ (red), and $\tau = 10000$ (black). *Left Column*: $R = 0.1$; *Middle Column*: $R = 1.0$; *Right Column*: $R = 10.0$. *Top Row*: Distribution in Δz; *Bottom Row*: Distribution in Δx.

The particle distributions (figure 5.13) for this model are also different from both the slab and 2D results in that the distributions can be described very well by a Gaussian function. The characteristic functions (figure 5.14), on the other hand, still show the fluctuations characteristic of the slab model in the parallel projection, and the longer decay of the 2D model in the perpendicular projection. The velocity correlation (figure 5.15) does show agreement with the theoretical assumption, similar to the slab model, and decays to zero. The comparison of the exact and approximate full velocity correlations (figures 5.16, 5.17) also show similarities to the pure slab and pure 2D correlations.

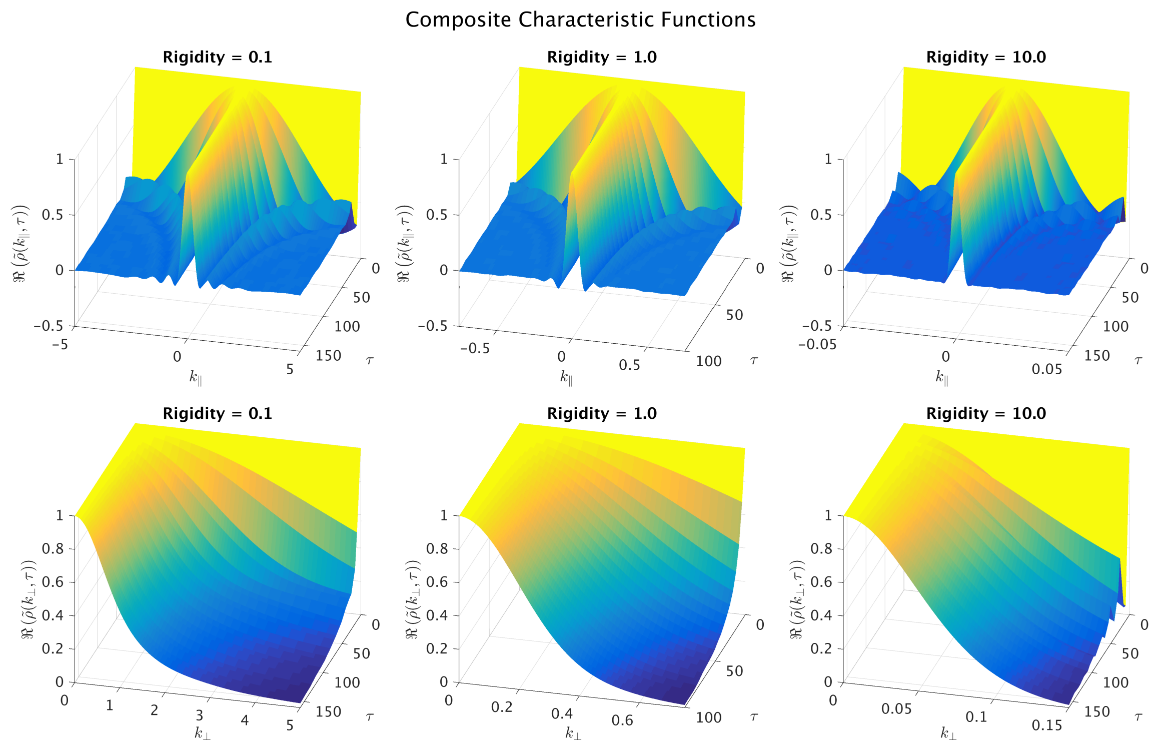

Figure 5.14: Real component of the characteristic functions $\tilde{\rho}(k_\parallel, \tau)$ and $\tilde{\rho}(k_\perp, \tau)$ for composite turbulence, model 1. *Left*: $R = 0.1$; *Center*: $R = 1.0$; *Right*: $R = 10.0$; *Top Row*: Parallel Component; *Bottom Row*: Perpendicular Component.

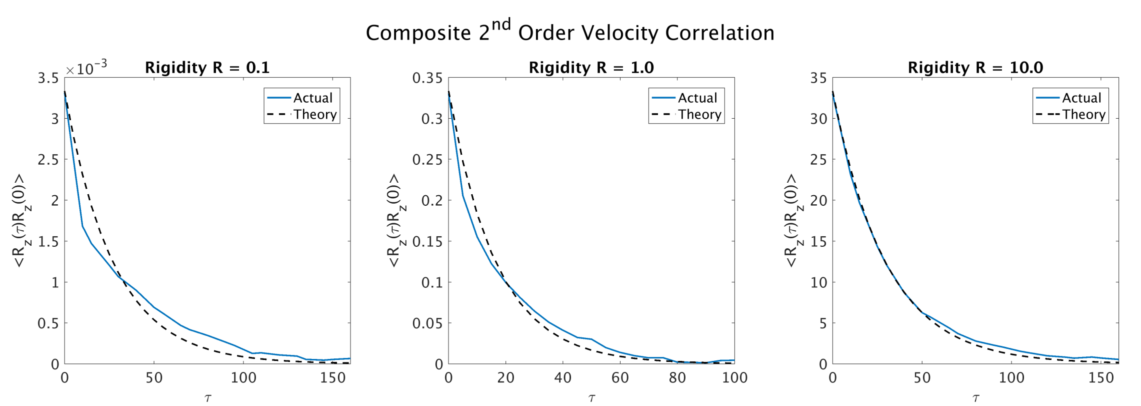

Figure 5.15: Second order velocity correlation (equation 2.43) for composite turbulence, model 1. The dashed line indicates the value of equation 2.43. *Left*: $R = 0.1$; *Center*: $R = 1.0$; *Right*: $R = 10.0$.

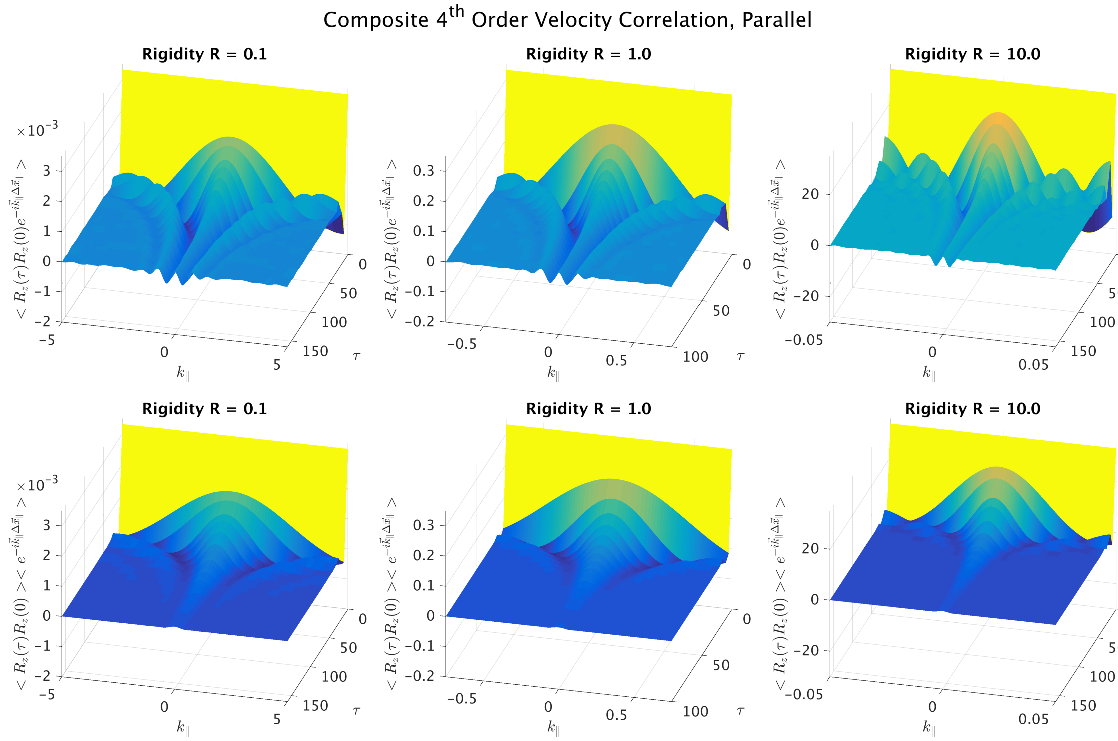

Figure 5.16: Comparison of the approximate and exact fourth order velocity correlation functions for composite turbulence, model 1. *Left Column*: $R = 0.1$; *Middle Column*: $R = 1.0$; *Right Column*: $R = 10.0$. *Top Row*: Exact Correlation; *Bottom Row*: Approximate Correlation.

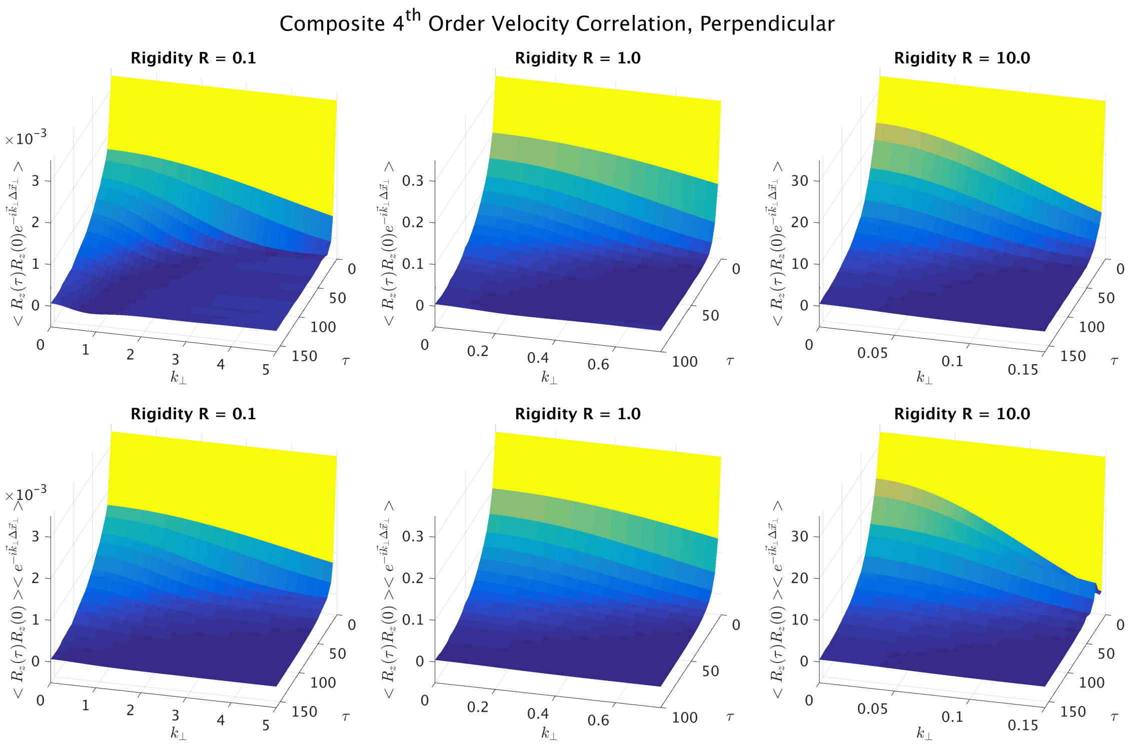

Figure 5.17: Comparison of the approximate and exact fourth order velocity correlation functions for composite turbulence, model 1. *Left Column*: $R = 0.1$; *Middle Column*: $R = 1.0$; *Right Column*: $R = 10.0$. *Top Row*: Exact Correlation; *Bottom Row*: Approximate Correlation.

5.4 Results for Composite Turbulence: Model 2

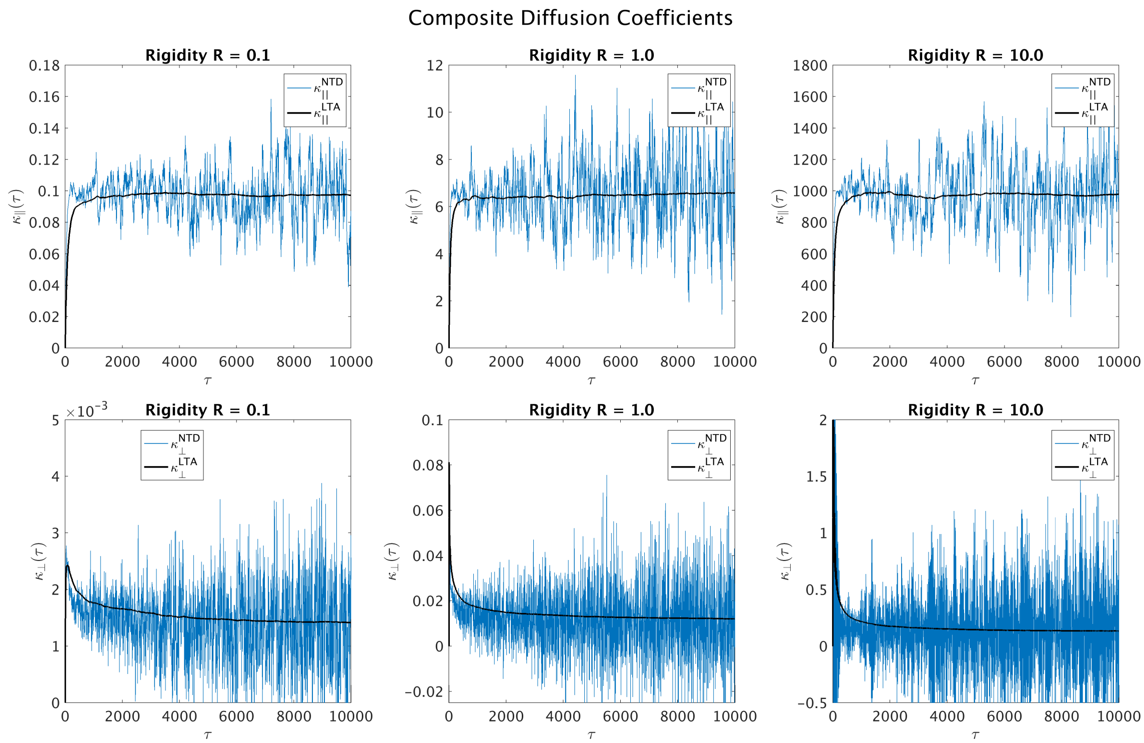

Figure 5.18: Diffusion coefficients for composite turbulence, model 2. *Right Column*: $R = 0.1$; *Middle Column*: $R = 1.0$ *Left Column*: $R = 10.0$; *Top Row*: Parallel Diffusion Coefficients; *Bottom Row*: Perpendicular Diffusion Coefficients.

When comparing the diffusion coefficients of this model (figure 5.18), we can see that the parallel diffusion coefficients given by the late time approximation are not just on the same order of magnitude, but also near the same value, with $\kappa_{\parallel}^{LTA}(R = 0.1) \approx 0.1$, $\kappa_{\parallel}^{LTA}(R = 1.0) \approx 6$, and $\kappa_{\parallel}^{LTA}(R = 10.0) \approx 10^3$. The perpendicular diffusion coefficients for this model, however, are less than half that of model 1. This difference also appears in the particle distributions (figure 5.19) as would be expected, and has the opposite affect on the characteristic functions (figure 5.23). The fluctuations in κ_{ii}^{NTD} are also larger in comparison to model 1.

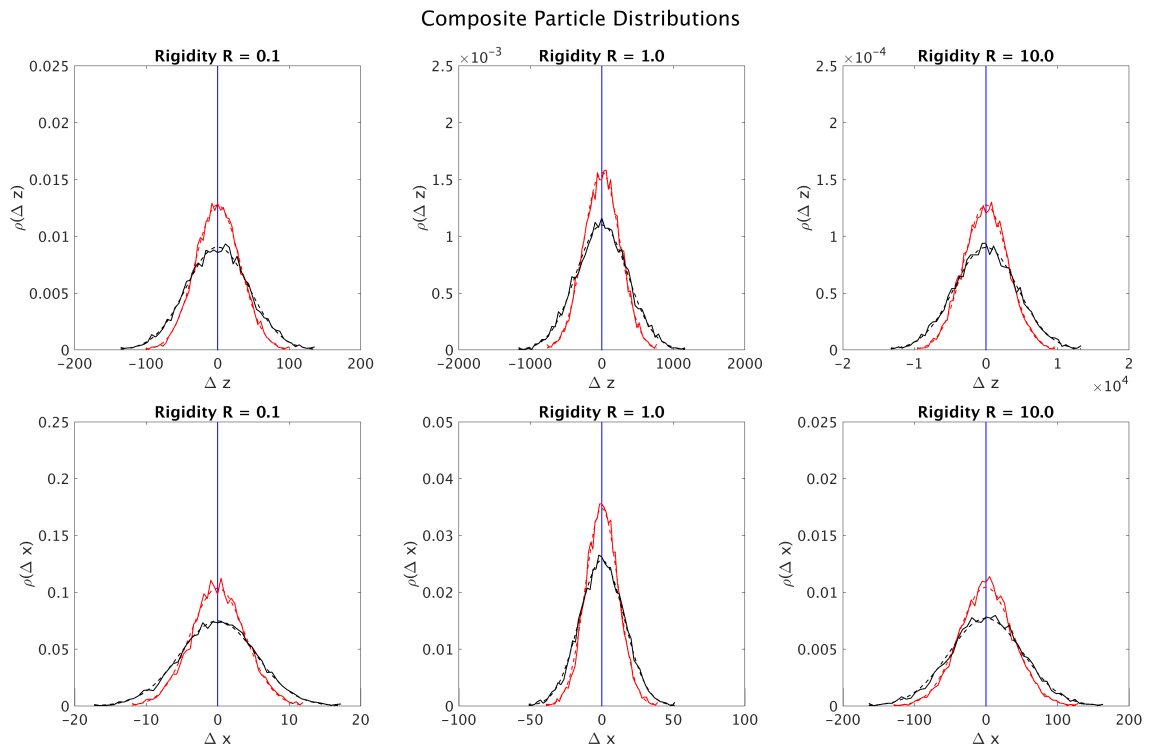

Figure 5.19: Particle distributions for composite turbulence, model 2. The dashed lines show the Gaussian distribution that results from the value of σ as calculated by equation 4.9. The times in each distribution are $\tau = 0$ (blue), $\tau = 5000$ (red), and $\tau = 10000$ (black). *Left Column*: $R = 0.1$; *Middle Column*: $R = 1.0$; *Right Column*: $R = 10.0$. *Top Row*: Distribution in Δz; *Bottom Row*: Distribution in Δx.

Similar to the first composite model, the density functions can easily be approximated by a Gaussian function, and the second order velocity correlation (figure 5.21) shows agreement between the actual velocity correlation and the exponential function used in theory. The characteristic functions and fourth order velocity correlations (figures 5.22, 5.23) also resemble the results from the first model.

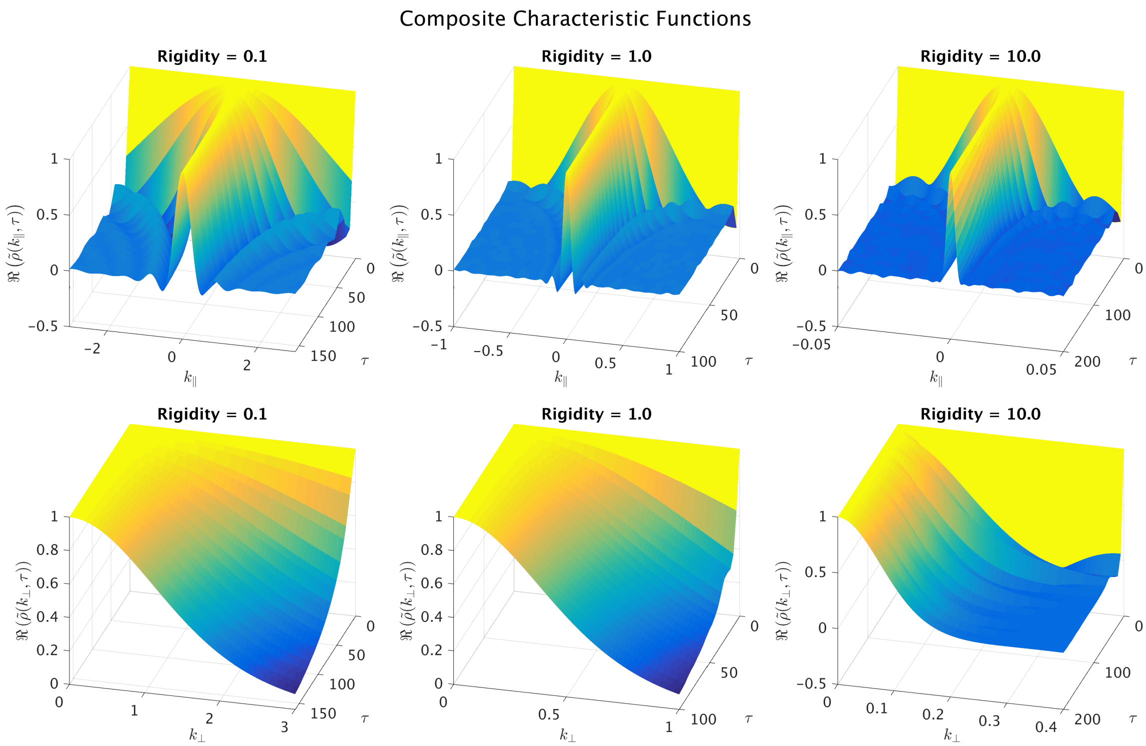

Figure 5.20: Real component of the characteristic functions $\tilde{\rho}(k_\parallel, \tau)$ and $\tilde{\rho}(k_\perp, \tau)$ for composite turbulence, model 2. *Left*: $R = 0.1$; *Center*: $R = 1.0$; *Right*: $R = 10.0$; *Top Row*: Parallel Component; *Bottom Row*: Perpendicular Component.

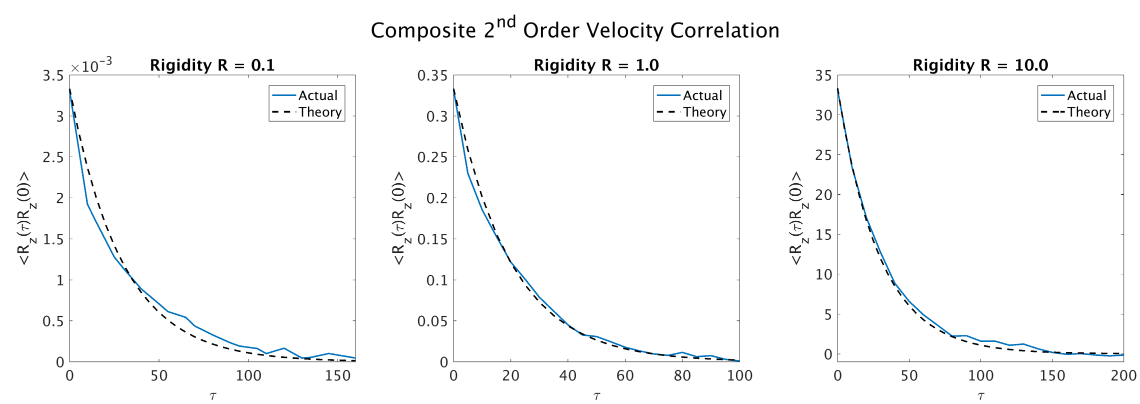

Figure 5.21: Second order velocity correlation (equation 2.43) for composite turbulence, model 2. The dashed line indicates the value of equation 2.43. *Left*: $R = 0.1$; *Center*: $R = 1.0$; *Right*: $R = 10.0$.

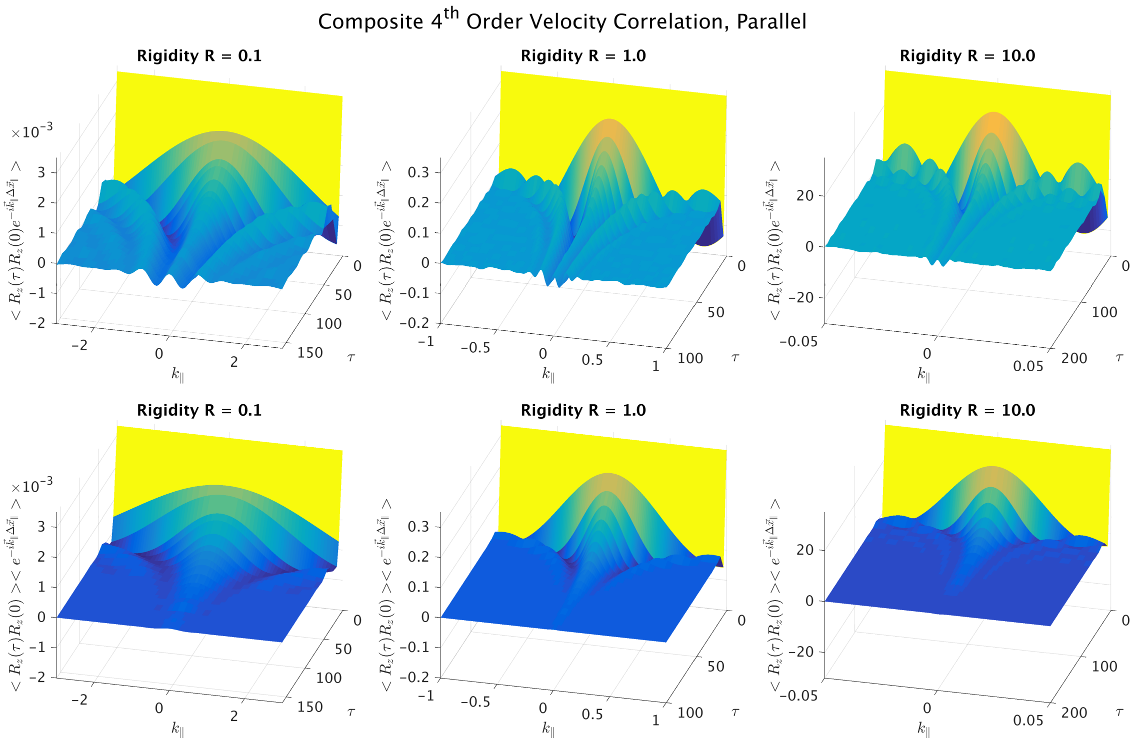

Figure 5.22: Comparison of the approximate and exact fourth order velocity correlation functions for composite turbulence, model 2. *Left Column*: $R = 0.1$; *Middle Column*: $R = 1.0$; *Right Column*: $R = 10.0$. *Top Row*: Exact Correlation; *Bottom Row*: Approximate Correlation.

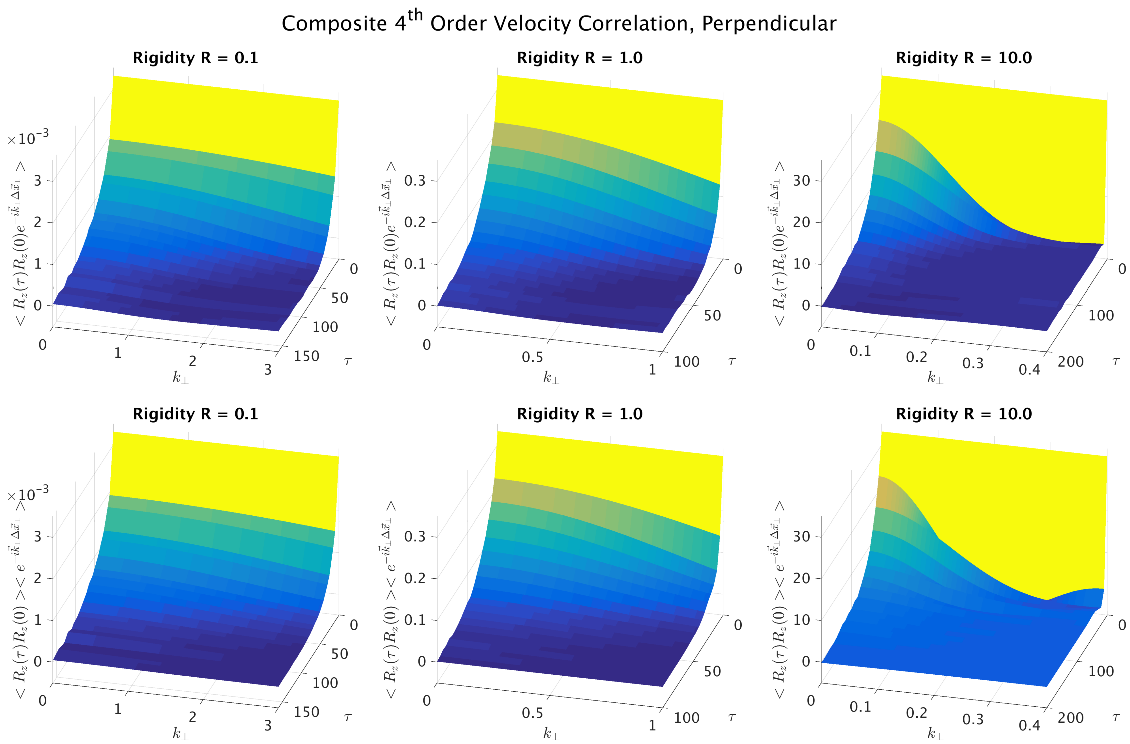

Figure 5.23: Comparison of the approximate and exact fourth order velocity correlation functions for composite turbulence, model 2. *Left Column*: $R = 0.1$; *Middle Column*: $R = 1.0$; *Right Column*: $R = 10.0$. *Top Row*: Exact Correlation; *Bottom Row*: Approximate Correlation.

5.5 Results for Composite Turbulence: Model 3

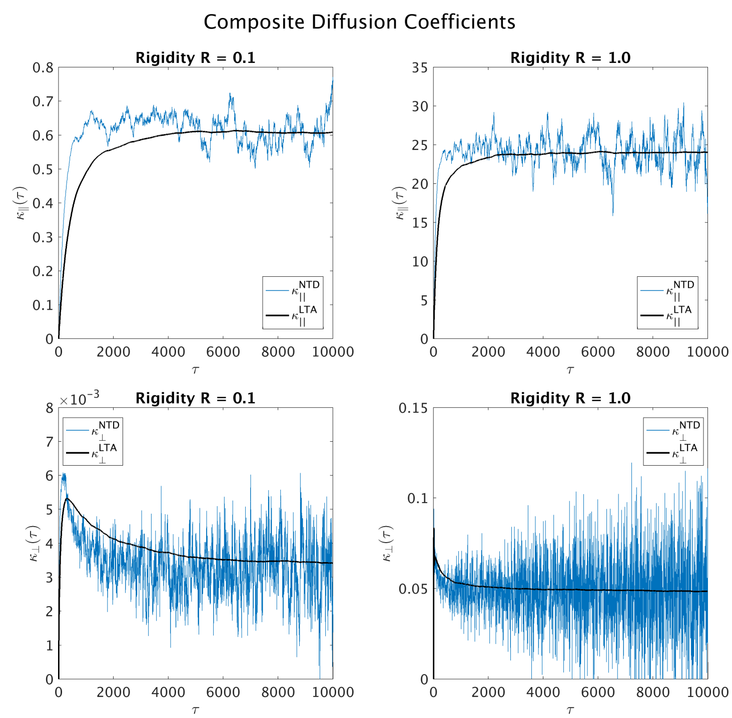

Figure 5.24: Diffusion coefficients for composite turbulence, model 3. *Right Column*: $R = 0.1$; *Left Column*: $R = 1.0$; *Top Row*: Parallel Diffusion Coefficients; *Bottom Row*: Perpendicular Diffusion Coefficients.

A comparison of the diffusion coefficients for the third composite model (figure 5.24) to the first composite model reveals that the parallel diffusion coefficients are larger for weaker turbulence. This is to be expected, as weaker turbulence means less force is applied to the particle, resulting in a smaller deflection of the particle trajectories away from the mean field. While this should mean that the perpendicular diffusion coefficients are smaller for this model, we find that $\kappa_{\perp}$ for $R = 0.1$ is roughly the same the first model, while $\kappa_{\perp}$ for $R = 1.0$ is around half the value for the first model. While the particle distribution functions (figure 5.25) resemble Gaussian distributions for $R = 1.0$, the distribution in Δx for $R = 0.1$ has a sharper peak

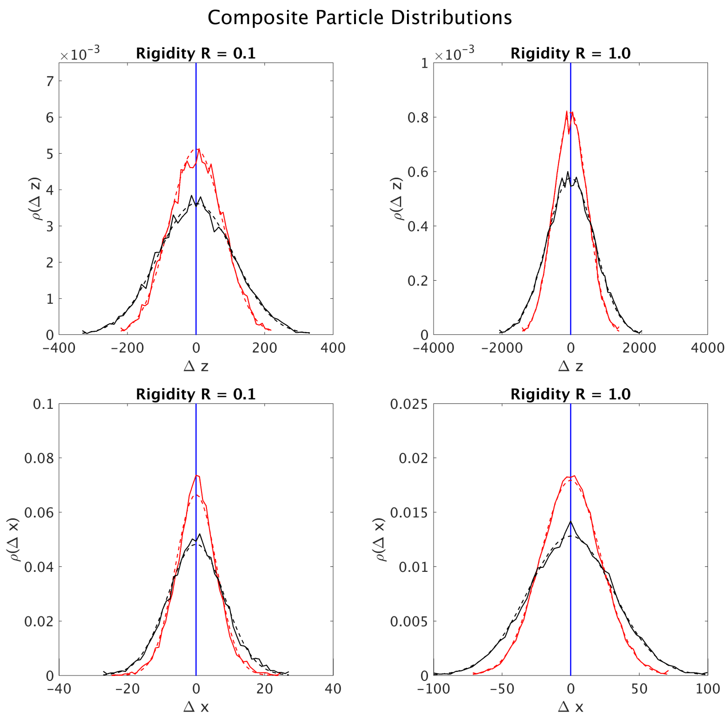

Figure 5.25: Particle distributions for composite turbulence, model 3. The dashed lines show the Gaussian distribution that results from the value of σ as calculated by equation 4.9. The times in each distribution are $\tau = 0$ (blue), $\tau = 5000$ (red), and $\tau = 10000$ (black). *Left Column*: $R = 0.1$; *Right Column*: $R = 1.0$. *Top Row*: Distribution in Δz; *Bottom Row*: Distribution in Δx.

than the overlay. The distribution in Δx for $R = 1.0$ at $\tau = 10^4$ also has a sharper peak to it. It is not certain whether this feature is due to the lower turbulence energy, or if it could be removed by increasing the particle count. As with the first and second composite models, the characteristic functions (figure 5.26) maintain the same general behaviour of the slab and 2D characteristic functions. Equation 2.43 describes the second order velocity correlation (figure 5.27) quite well, although the approximate fourth order velocity correlation does not match the exact fourth order velocity correlation (figure 5.28) for the parallel component. Without a qualitative analysis, it is not possible to draw any conclusions for the perpendicular fourth order correlation (figure 5.29) beyond that the exact correlation has a more well defined transition to a plateau.

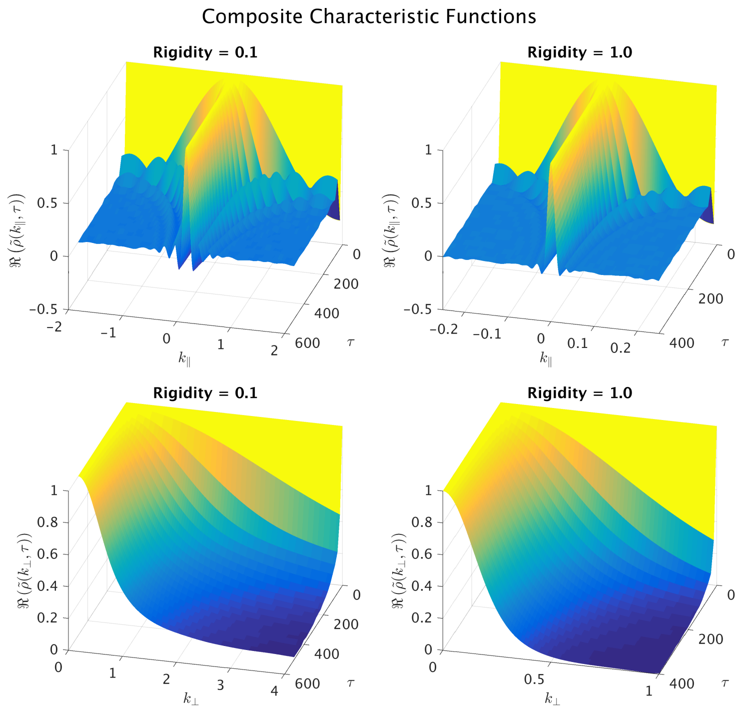

Figure 5.26: Real component of the characteristic functions $\tilde{\rho}(k_{\parallel}, \tau)$ and $\tilde{\rho}(k_{\perp}, \tau)$ for composite turbulence, model 3. *Left*: $R = 0.1$; *Right*: $R = 1.0$; *Top Row*: Parallel Component; *Bottom Row*: Perpendicular Component.

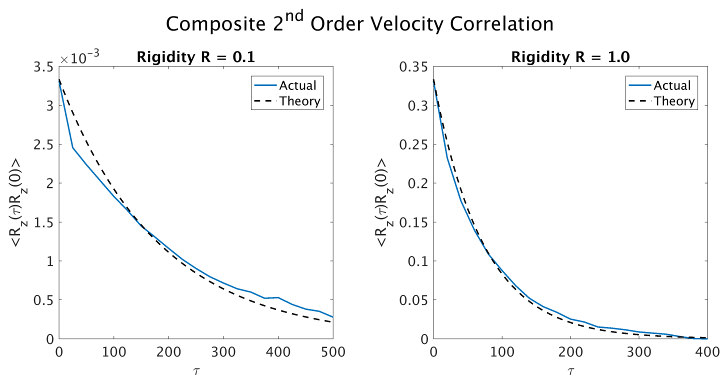

Figure 5.27: Second order velocity correlation (equation 2.43) for composite turbulence, model 3. The dashed line indicates the value of equation 2.43. *Left*: $R = 0.1$; *Right*: $R = 1.0$.

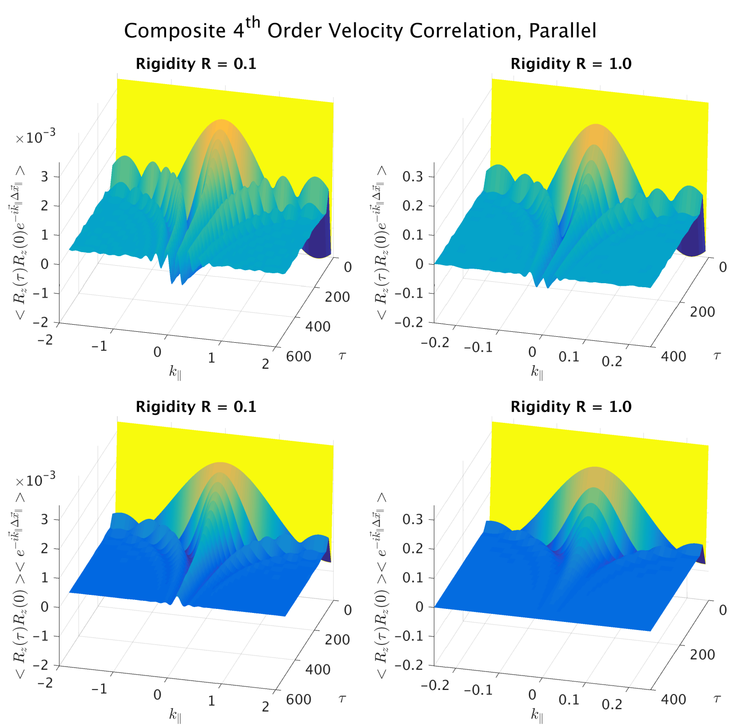

Figure 5.28: Comparison of the approximate and exact fourth order velocity correlation functions for composite turbulence, model 3. *Left Column*: $R = 0.1$; *Right Column*: $R = 1.0$. *Top Row*: Exact Correlation; *Bottom Row*: Approximate Correlation.

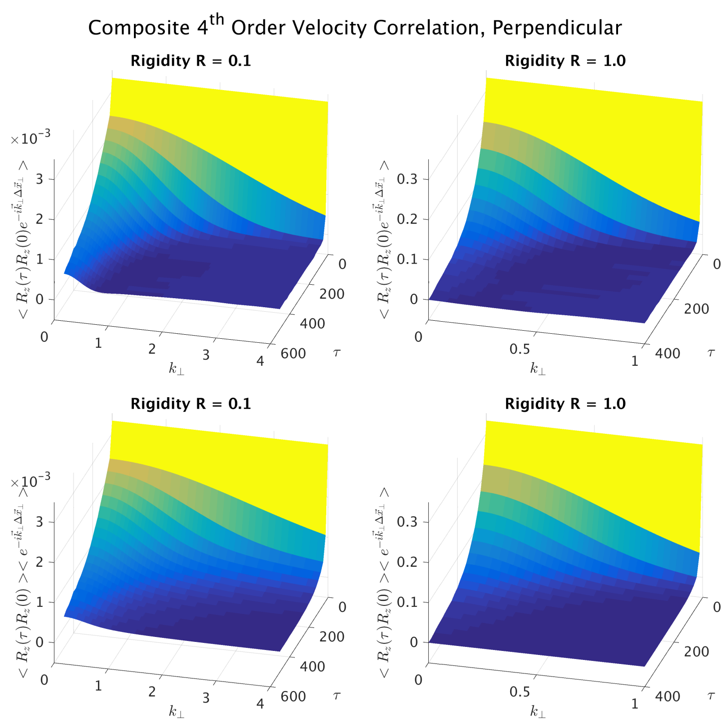

Figure 5.29: Comparison of the approximate and exact fourth order velocity correlation functions for composite turbulence, model 3. *Left Column*: $R = 0.1$; *Right Column*: $R = 1.0$. *Top Row*: Exact Correlation; *Bottom Row*: Approximate Correlation.

5.6 Results for Composite Turbulence: Model 4

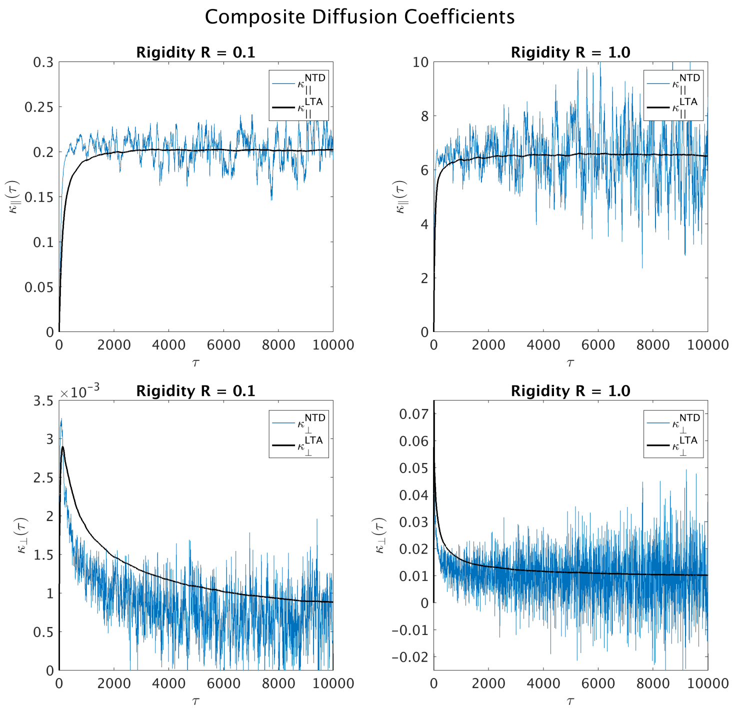

Figure 5.30: Diffusion coefficients for composite turbulence, model 4. *Right Column*: $R = 0.1$; *Left Column*: $R = 1.0$; *Top Row*: Parallel Diffusion Coefficients; *Bottom Row*: Perpendicular Diffusion Coefficients.

Instead of comparing this model to the first composite model, we use the third composite model as a reference, since both have the same total turbulent energy fraction. From figure 5.30, we can see that the diffusion coefficients are between three to four times smaller in this model than they are in model 3. Despite having the ratios of slab and 2D energy reversed, $\kappa_{\perp}^{NTD}$ indicates that the late time approximation will become diffusive at later times than what is simulated here. The particle densities (figure 5.31) are also similar to those of the third model, although the distribution in δx for $R = 0.1$ has a more noticeable deviation from the Gaussian overlay at the peak. The characteristic functions in figure 5.32, and fourth order velocity correlations (exact and approximate) in figures 5.34 and 5.35 show the same similarities as the other composite models to the constituent slab and 2D models that make up the composite turbulence. Equation 2.43 is again a decent description of the second order velocity correlation in figure 5.33.

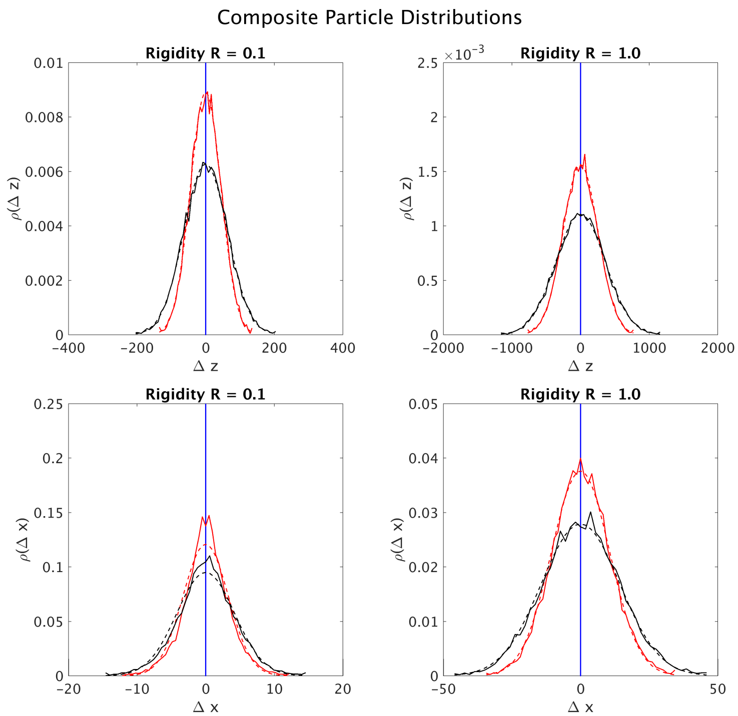

Figure 5.31: Particle distributions for composite turbulence, model 4. The dashed lines show the Gaussian distribution that results from the value of σ as calculated by equation 4.9. The times in each distribution are $\tau = 0$ (blue), $\tau = 5000$ (red), and $\tau = 10000$ (black). *Left Column*: $R = 0.1$; *Right Column*: $R = 1.0$. *Top Row*: Distribution in Δz; *Bottom Row*: Distribution in Δx.

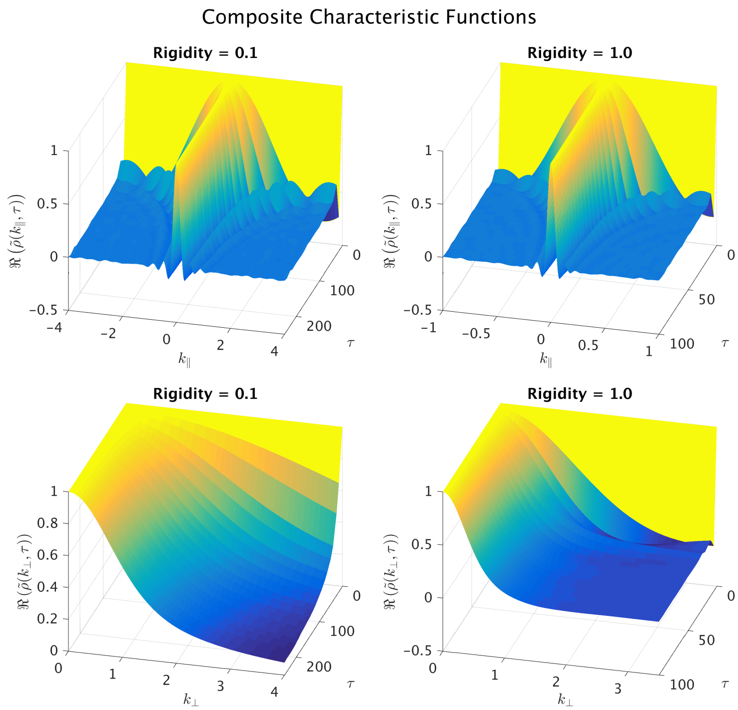

Figure 5.32: Real component of the characteristic functions $\tilde{\rho}(k_\parallel, \tau)$ and $\tilde{\rho}(k_\perp, \tau)$ for composite turbulence, model 4. *Left*: $R = 0.1$; *Right*: $R = 1.0$; *Top Row*: Parallel Component; *Bottom Row*: Perpendicular Component.

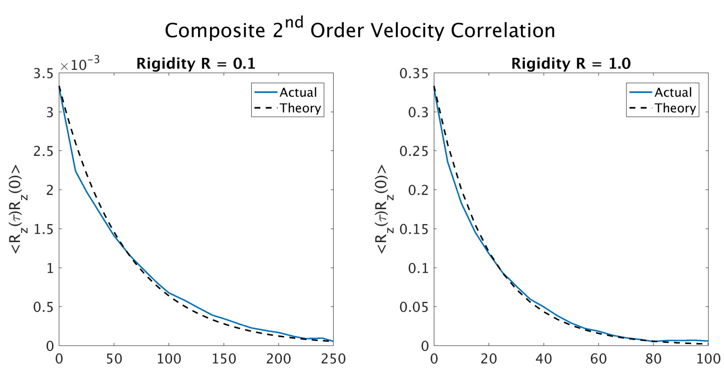

Figure 5.33: Second order velocity correlation (equation 2.43) for composite turbulence, model 4. The dashed line indicates the value of equation 2.43. *Left*: $R = 0.1$; *Right*: $R = 1.0$.

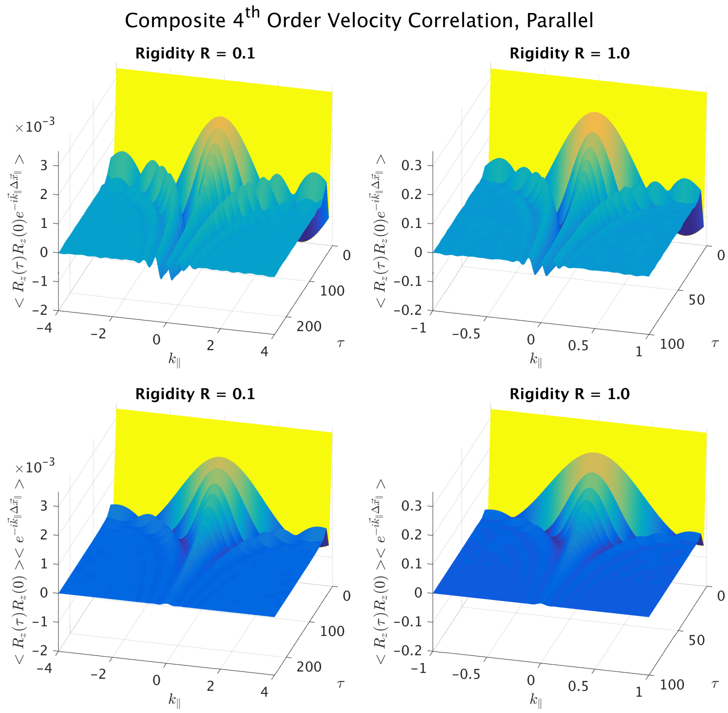

Figure 5.34: Comparison of the approximate and exact fourth order velocity correlation functions for composite turbulence, model 4. *Left Column*: $R = 0.1$; *Right Column*: $R = 1.0$. *Top Row*: Exact Correlation; *Bottom Row*: Approximate Correlation.

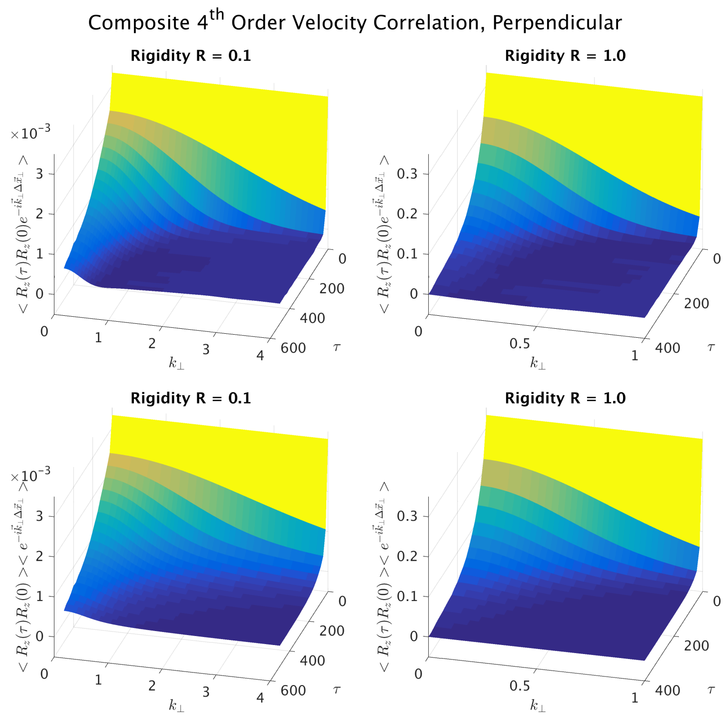

Figure 5.35: Comparison of the approximate and exact fourth order velocity correlation functions for composite turbulence, model 4. *Left Column*: $R = 0.1$; *Right Column*: $R = 1.0$. *Top Row*: Exact Correlation; *Bottom Row*: Approximate Correlation.

Chapter 6

Conclusions and Outlook

6.1 Summary of Results

In this thesis, we have discussed the transport of particles in turbulent magnetic environments in terms of a qualitative analysis of numerical simulations of particle trajectories. The assumption of a Gaussian distribution of particle displacements was tested, and the corresponding characteristic functions were calculated. A comparison of the theoretical approximation to the full velocity correlation with the exact results was carried out as well. Given the differences between the expectations from theory and the actual results from numerical work, it is hoped that this work will motivate the development of improved theories for cosmic ray transport. Presented here is a summary of the results for each of the quantities examined.

6.1.1 Diffusion Coefficients and Particle Distributions

The parallel diffusion coefficient for every model except the 2D model show diffusion within the simulation time, while the 2D results are inconclusive. The perpendicular diffusion coefficients were diffusive for the composite models, but sub-diffusive for the slab and 2D models within the given simulation time. The particle distributions for composite turbulence were found to be quite reasonably approximated by a Gaussian distribution, however the distributions for the slab and 2D turbulence models did not, with the distributions in Δx taking a different form altogether.

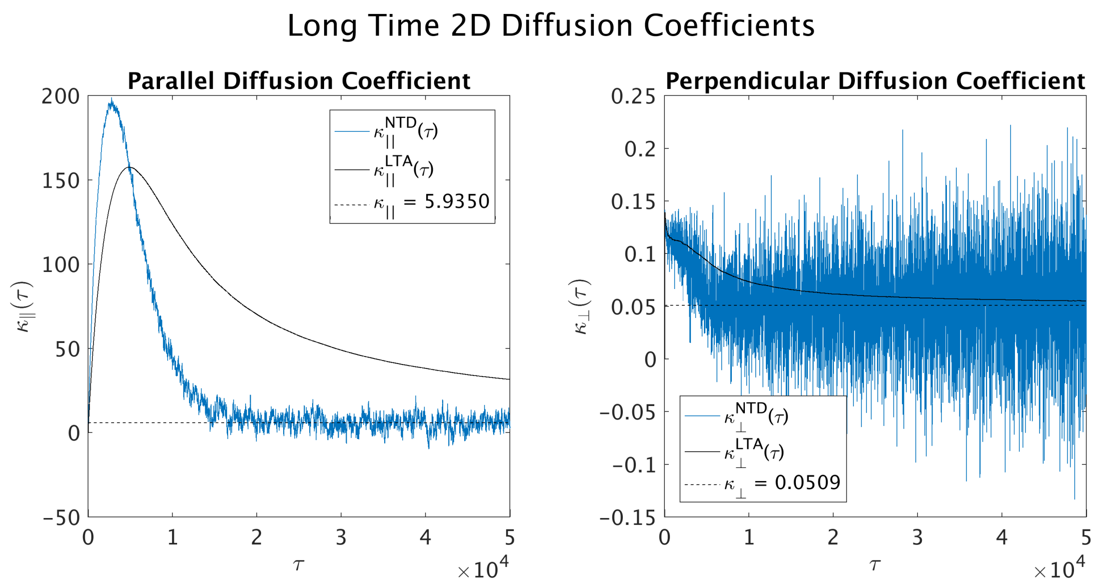

Figure 6.1: 2D diffusion coefficients after an extend period of time. The blue line is the NTD method (section 4.1.3), and the black line is the LTA method (section 4.1.1). The dashed red line is the average value of the NTD method for times greater than $2 \cdot 10^4$.

Given the behaviour of the diffusion coefficients in the 2D turbulence model, a simulation was run where the time was extended from $\tau_{max} = 10^4$ to $\tau_{max} = 5 \cdot 10^4$ to check whether or not diffusion can be achieved at all in the 2D models. Figure 6.1 shows the diffusion coefficients resulting from the simulation, using a rigidity of $R = 1.0$. By taking the average value of $\kappa_{ii}^{NTD}(\tau)$ for $2 \cdot 10^4 \leq \tau \leq 5 \cdot 10^4$, we can get an estimate of $\kappa_{ii} = \lim_{\tau \to \infty} \kappa_{ii}^{LTA}(\tau)$, shown by the dashed red line. The result is that both parallel and perpendicular transport asymptotically approach diffusive motion. This result also brings up the question as to whether the $R = 0.1$ diffusion coefficients require additional time to become diffusive, and is set to be the subject of future work.

6.1.2 Characteristic Functions

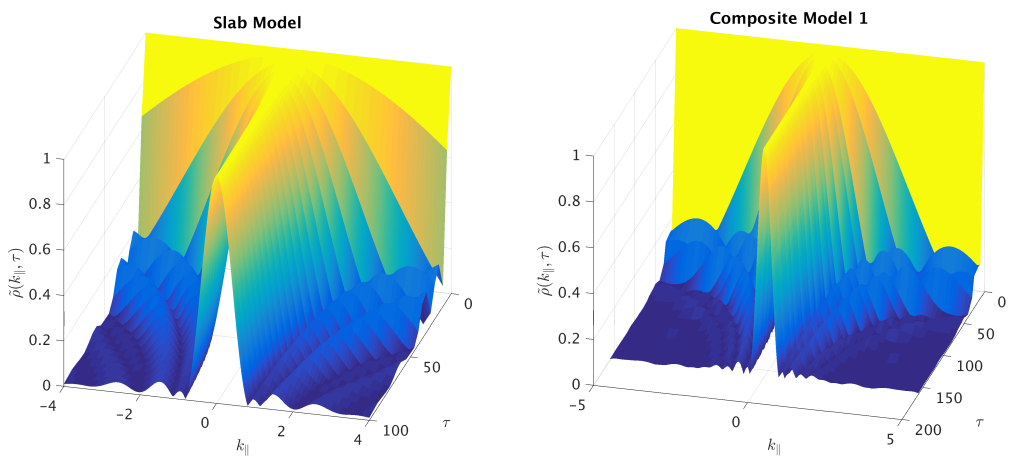

Figure 6.2: Absolute value of the parallel characteristic function for slab turbulence (*right*) and composite turbulence, model 1 (*left*). The rigidity used is $R = 0.1$.

The results for the characteristic functions can be divided into the parallel results and the perpendicular results. The parallel functions did not take the form of a Gaussian, even when the particle distributions did for the composite models. Instead they had additional oscillations as the wave number was increased. In section 5.1 it was speculated that this may be a result of the particles not having achieved diffusion at the times when the function was calculated, and since the distribution functions were calculated for times after diffusion had been achieved, it is not currently possible to state whether or not this is the case. It could be argued that the oscillations are the result of a non zero mean displacement, in which case the absolute value of the characteristic function would not have the oscillations. Figure 6.2 shows that the oscillations still exist when taking the absolute value.

6.1.3 Velocity Correlations

Except for the pure 2D model, it was found that equation 2.43 is a decent approximation for the second order velocity correlation. The parallel component of the full velocity correlation, however, cannot be approximated by the product of the normal velocity correlation and the characteristic function. Outside of a few cases where a difference could be seen around the change in the slope of the perpendicular velocity correlation, it is found to be difficult to draw qualitative conclusions about the relation between the approximate and exact perpendicular correlations. Further work will be required to give a quantitative analysis of any differences between these.

6.2 Future Work

The primary quantity used in calculating the results presented in this thesis is the particle's displacement vector, $\Delta\vec{x}(\tau) = \vec{x}(\tau) - \vec{x}(0)$. In the analysis methods we used, each particle provides one displacement vector for each point in time. However, it is possible to increase the number of particle trajectories, and thereby increase the number of displacement vectors, by removing the condition that $\tau_0 = 0$. The rationalization for this change can be summarized as follows:

- The turbulence models used do not depend on time, therefore the particle trajectories only depend on where they start, not when they start.

- Since the trajectory of a particle does not depend on the value of τ_0, the trajectories are left unchanged by any shift in time. This means that the particle position and momentum at any specific point in time τ_n is a valid starting point for another particle trajectory.

- These new particles will follow the exact same path as the original particles, giving a new trajectory that is tracked for a duration of time given by $\tau'_{max} = \tau_{max} - \tau_n$.

The effect of this change is that the number of particle trajectories available for a given point in time τ_n is increased by a factor of $(nT - 1) - n$, where nT is the total number of points in time that are output by the simulation. This method allows for a large increase in statistical counts for times not near the end of the simulation at no additional cost in total time required to generate the trajectories. Instead, the additional run time is shifted to the analysis of the results. This method would not be applicable to simulations where electric fields are included, and it is unclear whether it would be valid for dynamic turbulence as well. Still any future work done with static turbulence stands to benefit from this method of analysis.

Beyond a re-implementation of the analysis methods, several other opportunities to build on this work are available. Some of these are:

- A quantitative analysis of the differences between the exact full velocity correlation and its approximation.
- A further study of particle behaviour in two dimensional turbulence after extended periods of time.
- The calculation and characterization of the drift coefficients for different turbulence models.
- The use of dynamic magnetic turbulence and the calculation of the full velocity correlation (exact and approximate).

- A test of whether Corrsin's hypothesis is valid, and a characterization of any differences between the full velocity-magnetic field correlation and the approximation used in the hypothesis.

- The inclusion of electrical fields in simulations for the study of momentum diffusion. This requires a rework of the integration method, as it is currently incapable of handling changes in the magnitude of the velocity.

Bibliography

Arendt, V. and A. Shalchi (2018, June). Time-dependent transport of energetic particles in magnetic turbulence: computer simulations versus analytical theory. Ap&SS *363*, 116.

Bieber, J. W., W. H. Matthaeus, C. W. Smith, W. Wanner, M.-B. Kallenrode, and G. Wibberenz (1994, January). Proton and electron mean free paths: The Palmer consensus revisited. ApJ *420*, 294–306.

Bieber, J. W., W. Wanner, and W. H. Matthaeus (1996, February). Dominant two-dimensional solar wind turbulence with implications for cosmic ray transport. J. Geophys. Res. *101*, 2511–2522.

Corrsin, S. (1959). Progress Report on Some Turbulent Diffusion Research. Adv. Geophys. *6*, 161.

Dröge, W. (2000, July). Particle Scattering by Magnetic Fields. Space Sci. Rev. *93*, 121–151.

Earl, J. A. (1974, October). The diffusive idealization of charged-particle transport in random magnetic fields. ApJ *193*, 231–242.

Fletcher, L. (1997, October). Numerical simulations of coronal particle trapping. A&A *326*, 1259–1267.

Green, M. S. (1951, August). Brownian Motion in a Gas of Noninteracting Molecules. J. Chem. Phys. *19*, 1036–1046.

Heusen, M. H. (2017). *Analytical and numerical investigation of energetic particles interacting with turbulent magnetic fields*. Ph. D. thesis, University of Manitoba.

Hussein, M., R. C. Tautz, and A. Shalchi (2015, June). The influence of different turbulence models on the diffusion coefficients of energetic particles. J. Geophys. Res. *120*, 4095–4111.

Jokipii, J. R. (1966, November). Cosmic-Ray Propagation. I. Charged Particles in a Random Magnetic Field. ApJ *146*, 480.

Kronberg, P. P. and R. V. E. Lovelace (2015, August). Extragalactic circuits, transmission lines, and CR particle acceleration. In *European Physical Journal Web of Conferences*, Volume 99 of *European Physical Journal Web of Conferences*, pp. 13005.

Kubo, R. (1957, June). Statistical-Mechanical Theory of Irreversible Processes. I. J. Phys. Soc. Jpn. *12*, 570–586.

Lasuik, J. and A. Shalchi (2017a, October). Solutions of the cosmic ray velocity diffusion equation. Adv. Space Res. *60*, 1532–1546.

Lasuik, J. and A. Shalchi (2017b, September). Time-dependent Perpendicular Transport of Energetic Particles for Different Turbulence Configurations and Parallel Transport Models. ApJ *847*, 9.

Malkov, M. A. and L. O. Drury (2001, April). Nonlinear theory of diffusive acceleration of particles by shock waves. Rep. Prog. Phys. *64*, 429–481.

Matthaeus, W. H., M. L. Goldstein, and D. A. Roberts (1990, December). Evidence for the presence of quasi-two-dimensional nearly incompressible fluctuations in the solar wind. J. Geophys. Res. *95*, 20673–20683.

Matthaeus, W. H., G. Qin, J. W. Bieber, and G. P. Zank (2003, June). Nonlinear Collisionless Perpendicular Diffusion of Charged Particles. ApJ *590*, L53–L56.

Pierre Auger Collaboration, J. Abraham, P. Abreu, M. Aglietta, C. Aguirre, D. Allard, I. Allekotte, J. Allen, P. Allison, C. Alvarez, and et al. (2007, November). Correlation of the Highest-Energy Cosmic Rays with Nearby Extragalactic Objects. *Science 318*, 938.

Schlickeiser, R. (2002). *Cosmic Ray Astrophysics*. Springer.

Shalchi, A. (2009). *Nonlinear Cosmic Ray Diffusion Theories*, Volume 362 of *Astrophysics and Space Science Library*. Springer.

Shalchi, A. (2010, September). A Unified Particle Diffusion Theory for Cross-field Scattering: Subdiffusion, Recovery of Diffusion, and Diffusion in Three-dimensional Turbulence. ApJ *720*, L127–L130.

Shalchi, A. (2017, May). Time-dependent perpendicular transport of energetic particles in magnetic turbulence with transverse complexity. Phys. Plasmas *24*(5), 050702.

Shalchi, A. and B. Weinhorst (2009, May). Random walk of magnetic field lines: Subdiffusive, diffusive, and superdiffusive regimes. Adv. Space Res. *43*, 1429–1435.

Tautz, R. C. (2010, January). A new simulation code for particle diffusion in anisotropic, large-scale and turbulent magnetic fields. Comput. Phys. Commun. *181*, 71–77.

Taylor, G. I. (1922). Diffusion by continuous movements. P. Lond. Math. Soc. *s2-20*(1), 196–212.

Webb, G. M., G. P. Zank, E. K. Kaghashvili, and J. A. le Roux (2006, November). Compound and Perpendicular Diffusion of Cosmic Rays and Random Walk of the Field Lines. I. Parallel Particle Transport Models. ApJ *651*, 211–236.

Yoshida, H. (1992). Symplectic Integrators for Hamiltonian Systems: Basic Theory. In S. Ferraz-Mello (Ed.), *Chaos, Resonance, and Collective Dynamical Phenomena in the Solar System*, Volume 152 of *IAU Symposium*, pp. 407.